

On a stress resultant geometrically exact shell model. Part V. Nonlinear plasticity: formulation and integration algorithms*

J.C. Simo and J.G. Kennedy

Division of Applied Mechanics, Department of Mechanical Engineering, Stanford University,
Stanford, California, USA

Received 28 March 1989

Revised manuscript received 20 January 1991

The continuum basis and numerical implementation of a finite deformation plasticity model formulated within the framework of the geometrically exact shell model presented in Parts I and III of this work, is discussed in detail. The model is formulated entirely in *stress resultants*, and hence the expensive integration through the thickness associated with the traditional degenerated solid approach is entirely by-passed. In particular, the classical Ilyushin–Shapiro plasticity model for shells is extended to accommodate kinematic and isotropic hardening, and consistently formulated to accommodate finite deformation. The corresponding closest-point-projection return mapping algorithm is shown to reduce to the solution of a system of two nonlinear scalar equations, and proved to be amenable to exact linearization leading to a closed form expression of the *consistent* elastoplastic tangent moduli. Numerical simulations are presented and comparisons with exact and approximate solutions are made which demonstrate the excellent performance of the proposed methodology.

1. Introduction

In Parts I, II and III of this work, we have presented the formulation, numerical analysis and implementation of a nonlinear shell theory formulated entirely in terms of stress resultants. This theory thus falls within the realm of ‘classical’ shell models, which are typically formulated in stress resultants (and stress couples). It is by now well known that the momentum equations of shell theory (formulated in stress resultants) take a canonical (or generic) form which is, in fact, independent of the method of derivation. The general structure of the constitutive equations in shell theory is also known in the specific case of elastic response. A main thrust of our previous work has been to demonstrate that these canonical equations can be reformulated in a form which circumvents the apparent complexities found in classical expositions of the subject, and is directly amenable to numerical implementation.

From an engineering perspective, however, if stress resultant shell theories are to become a standard engineering tool that replaces the widely used *continuum degenerated solid approach*, the crucial issue that remains to be addressed concerns the formulation and implementation of inelastic constitutive models. Two different approaches can be adopted: (i) use of three-dimensional plasticity models and numerical computation of the stress resultants and stress couples by integration through the thickness of the shell, or (ii) use of constitutive models formulated *directly in stress resultants*.

* Research supported by AFOSR under contract numbers 2-DJA-544 and 2-DJA-771 with Stanford University.

The *through-the thickness pre-integrated* approach has been advocated by Stanley [1], among others, and represents a step forward in the simplification of the traditional solid formulation. Note, however, that the balance laws should remain formulated in resultants, in contrast with typical formulations adopting this approach, including that of Stanley [1]. The advantages of this method are as follows:

- (ia) Conceptual simplicity is inherited from the three-dimensional theory.
- (ib) Direct applicability of existing three-dimensional constitutive models is maintained. For plasticity, for instance, this leads to the use of the standard return mapping algorithms, see e.g. [2] for a review.

There are, however, two major disadvantages associated with this widely used approach:

- (ic) Computational cost: even if the balance laws are formulated in terms of stress resultants, a numerical integration through the thickness is required to compute the stress resultants.
- (id) Prevalence of rate formulations of the ‘stress-strain’ equation in terms of objective stress rates. In this type of shell theory, rate formulations are used as a means of enforcing constraints present in shell theory on the constitutive model; in particular, the plane-stress assumption. As a result, *objective integration algorithms* are required to define the elastic predictor (trial stress); see [2, Chapter 7]. This leads to added cost in the formulation, and precludes the desirable use of the so-called *algorithmic tangent moduli* [3].

In the second approach, which has not been widely used in the literature until recently, constitutive models are formulated *directly in stress-resultants*. An example of this approach is the work of Crisfield [4, 5]. The primary advantage of this methodology lies in the following feature:

- (iia) Computational cost: in this approach, the integration through the thickness associated with the degenerated solid formulation is entirely eliminated from the computational procedure.

This reduction in cost, however, is accomplished at the expense of introducing considerably more complex functional forms in the constitutive response functions. For elastoplasticity, for instance, even the simplest yield criterion; e.g., the Von Mises condition, leads to a rather complex functional form when expressed in stress resultants, as is demonstrated in the classical work of Ilyushin [6], Shapiro [7] and Ivanov [8]. These yield criteria often exhibit a lack of regularity which, from an algorithmic point of view, requires a careful treatment. To summarize, the disadvantages of this second approach are as follows:

- (iib) Implementation of three-dimensional material models may prove to be a difficult task. It is not a priori clear how to perform a closed-form, analytical reduction of complex three-dimensional constitutive models to resultant form.
- (iic) The complexity of the algorithmic treatment is typically increased. For elastoplasticity, for instance, the formulation and implementation of proper return mapping algorithms for models with general yield surfaces intersecting in a possibly nonsmooth fashion is not a trivial task.

Despite the aforementioned shortcomings, we believe that the low cost advantage more than offsets the difficulties associated with this latter approach.

The objective of this paper is to present a rather general treatment of plasticity, in the context of shell theory, for constitutive models formulated in stress resultants. Our contributions, we believe, lie in the following features.

- (1) The formulation discussed herein is completely general, at least within the context the classical kinematic assumption of shell theory that straight fibers off the mid-surface remain straight, and is not restricted to the case of infinitesimal kinematics. That is, all kinematic quantities such as the displacements, rotations and strains may be large. Of course, the utility

of the classical kinematic assumption degrades as the transverse shear and membrane strains become large, but this speaks of the underlying shell theory itself and not the current formulation of that theory.

We illustrate the theory by means of a properly invariant extension of the classical Ilyushin–Shapiro yield condition for J_2 -flow theory.

(2) Our extension of the Ilyushin–Shapiro plasticity model to the nonlinear theory includes both *kinematic* and *isotropic* hardening. The flow rule is *associative* leading, therefore, to symmetric tangent moduli. Accordingly, the model constitutes the counterpart in *nonlinear* shell theory of the classical J_2 -flow theory with kinematic/isotropic hardening.

(3) Within the framework of our previous work on multi-surface plasticity [9], we construct an unconditionally stable return mapping algorithm which, at the stress-point level, involves only the solution of *two nonlinear* scalar equations. This algorithm is amenable to exact linearization leading to a closed-form expression for the consistent elastoplastic tangent moduli.

(4) In the proposed formulation, the elastic response emanates from a hyperelastic form of the free energy function, an example of which is discussed. The elastic predictor is therefore exact, and is computed without resorting to *incrementally objective* algorithms.

An outline of the paper is as follows. In Section 2 we give an account of the basic kinematics, strain measures and rate of deformation tensors employed in the formulation of the general theory. The structure of the general elastoplastic model is outlined in Section 3, and the concrete application to a model of the Ilyushin–Shapiro type is undertaken in Section 4. In Section 5 we give an explicit construction of the return mapping algorithm. Numerical simulations which illustrate the performance of the proposed formulation, including comparisons with available solutions and large-scale simulations exhibiting very large deformations, are given in Section 6. Details pertaining to the linearization of the algorithm and the thermodynamic structure of the theory are given in two appendices.

We close this introduction with a remark on our finite element implementation. In our previous work of Parts II and III, we have employed a mixed (*assumed-stress*) finite element method for the membrane and bending fields based on a Hellinger–Reissner variational formulation. Conceptually, the extension of this computational framework to accommodate elastoplastic response follows identical lines to those considered in detail by Simo et al. [10]. For simplicity, however, we have chosen to present the methodology developed herein within the much simpler and classical context of a strain-driven method. In particular, our numerical simulations employ a *nonoptimal* displacement formulation for the membrane and bending field. Recently, however, we have constructed an *assumed stress* method which inherits similar accuracy properties for coarse meshes as our previous assumed stress formulation without the need to modify the return mapping algorithm at the stress-point level. We defer the discussion of this method to a subsequent publication. The assumed strain framework presented in Part III for the transverse shear strains, on the other hand, will be used here (i.e. the shear strains are linearly interpolated between mid-side nodes).

2. Kinematic relations: summary of field equations

In this section we examine in detail the geometric structure and alternative definitions of the strain measures, rates-of-deformation tensors, and stress resultants associated with the geometrically exact shell model considered in Parts I and III of this work. These notions, which were not discussed in depth in our previous work, play a central role in the

formulation of inelastic constitutive equations. For further details on this and related topics we refer to Simo and Fox [11], and Simo et al. [12, 13].

2.1. Configurations: kinematic description of the shell

Following Parts I and III of this work, we recall that from a geometric standpoint, a shell-like body is described in terms of the following two objects (see Fig. 1):

- (i) The *mid-surface* of the shell, viewed as a parametrized surface; that is, as a map $\varphi: \mathcal{A} \rightarrow \mathbb{R}^3$, where $\mathcal{A} \subset \mathbb{R}^2$ is the domain of the parameterization; a compact set with smooth boundary $\partial\mathcal{A}$ and points denoted by $\xi := (\xi^1, \xi^2) \in \bar{\mathcal{A}} := \mathcal{A} \cup \partial\mathcal{A}$. In the context of the finite element method, this parameterization is defined by a collection of charts constructed via the iso-parametric mapping. We denote by

$$\mathcal{S} := \{\bar{x} = \varphi(\xi) \mid \xi \equiv (\xi^1, \xi^2) \in \bar{\mathcal{A}}\}, \quad (2.1)$$

the actual mid-surface; i.e., the graph of φ .

- (ii) The *director field* of the shell, viewed as a vector field $\bar{t}: \mathcal{S} \rightarrow S^2$ which assigns to each point $\bar{x} \in \mathcal{S}$ of the mid-surface a vector $\bar{t}(\bar{x}) \in S^2$. Here, S^2 denotes the unit sphere defined as

$$S^2 := \{t \in \mathbb{R}^3 \mid \|t\| = 1\}. \quad (2.2)$$

As in Part I, we parametrize the director field by the map $t := \bar{t} \circ \varphi: \mathcal{A} \rightarrow S^2$ ¹.

With these two objects in hand, the kinematic assumption underlying the shell model under consideration is that *any* placement of the shell in Euclidean space, denoted by $\mathcal{B} \subset \mathbb{R}^3$, is given as

$$\mathcal{B} := \{x \in \mathbb{R}^3 \mid x = \varphi + \xi t \text{ where } (\varphi, t) \in \mathcal{C} \text{ and } \xi \in [h^-, h^+]\}, \quad (2.3)$$

where $[h^-, h^+] \subset \mathbb{R}$ with $h^+ > h^-$ is interpreted as the thickness of the shell, and \mathcal{C} is the manifold of admissible parameterizations of the mid-surface and the director field; i.e.,

$$\mathcal{C} := \{\Phi := (\varphi, t): \bar{\mathcal{A}} \subset \mathbb{R}^2 \rightarrow \mathbb{R}^3 \times S^2 \mid t \cdot \varphi_{,1} \times \varphi_{,2} > 0 \text{ and } \|\varphi_{,1} \times \varphi_{,2}\| \neq 0\}. \quad (2.4)$$

Note that the conditions appended to (2.4) preclude the physically unreasonable situation of

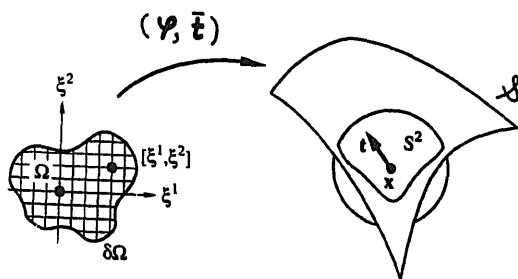


Fig. 1. Illustration of the geometry which defines the kinematics of the shell model.

¹ As shown in Part IV of this work, the inextensibility constraint requiring that $t \in S^2$ can be easily removed. We introduce this assumption here only for simplicity.

infinite transverse shear deformation, and require regularity of the parameterization. In terms of the unit vector field $\bar{\nu}: \mathcal{S} \rightarrow S^2$ normal to the mid-surface, with parameterization $\nu := \bar{\nu} \circ \varphi$ defined as

$$\nu := \frac{\mathbf{a}_1 \times \mathbf{a}_2}{\|\mathbf{a}_1 \times \mathbf{a}_2\|}, \quad \text{where } \mathbf{a}_\alpha := \varphi_\alpha, \quad (2.5)$$

these two requirements are equivalent to the conditions that

$$\nu \neq 0 \quad \text{and} \quad t \cdot \nu > 0. \quad (2.6)$$

Consequently, at each point $\bar{x} \in \mathcal{S}$ we have the well-defined frame $\{\mathbf{a}_1, \mathbf{a}_2, \mathbf{t}\}$ called the *natural frame*. We denote by $a_{\alpha\beta}$ the components of the induced Riemannian metric (i.e., the first fundamental form) and set²

$$a_{\alpha\beta} := \mathbf{a}_\alpha \cdot \mathbf{a}_\beta \quad \text{and} \quad \gamma_\alpha := \mathbf{a}_\alpha \cdot \mathbf{t}. \quad (2.7)$$

The *reciprocal* or *covariant* natural frame, denoted by $\{\mathbf{a}^1, \mathbf{a}^2, \mathbf{a}^3\}$, is then defined by the standard expressions

$$\mathbf{a}^3 \cdot \mathbf{a}_\alpha = \delta_\alpha^\beta, \quad \mathbf{a}^\alpha \cdot \mathbf{t} = 0, \quad \mathbf{a}^3 \cdot \mathbf{t} = 0 \quad \text{and} \quad \mathbf{a}^3 \cdot \mathbf{a}_\alpha = 0. \quad (2.8)$$

It is clear from the preceding discussion that, by virtue of the kinematic assumption, a given map $\Phi := (\varphi, \mathbf{t})$ in \mathcal{C} uniquely defines a placement of the shell. Accordingly, one refers to \mathcal{C} as the *abstract configuration space*. Boundary conditions of place are appended to definition (2.3) by requiring that

$$\varphi = \tilde{\varphi} \quad \text{on } \partial_\varphi \mathcal{A} \quad \text{and} \quad \mathbf{t} = \tilde{\mathbf{t}} \quad \text{on } \partial_t \mathcal{A}, \quad (2.9)$$

for any $\Phi := (\varphi, \mathbf{t}) \in \mathcal{C}$. Here $\partial_\varphi \mathcal{A}$ and $\partial_t \mathcal{A}$ are disjoint parts of the boundary $\partial \mathcal{A}$ such that $\overline{\partial_\varphi \mathcal{A} \cup \partial_t \mathcal{A}} = \partial \mathcal{A}$. We recall that \mathcal{C} is a differentiable manifold with tangent space at $\Phi \in \mathcal{C}$ denoted by $T_\Phi \mathcal{C}$ and defined by

$$T_\Phi \mathcal{C} = \{\delta\Phi := (\delta\varphi, \delta\mathbf{t}): \mathcal{A} \rightarrow \mathbb{R}^3 \times T_x S^2 \mid \delta\varphi|_{\partial_\varphi \mathcal{A}} = \mathbf{0} \text{ and } \delta\mathbf{t}|_{\partial_t \mathcal{A}} = \mathbf{0}\}. \quad (2.10)$$

As in Part I we adopt the following convention. We denote by \mathcal{B}^0 the *reference placement* of the shell, we let \mathcal{S}^0 be its *reference mid-surface*, and denote by $\{\mathbf{a}_1^0, \mathbf{a}_2^0, \mathbf{t}^0\}$ the reference natural frame. In general, unless otherwise explicitly stated, a superscript ‘0’ will refer to an object associated with the reference placement \mathcal{B}^0 .

Finally, we denote by $\{\mathbf{e}_1, \mathbf{e}_2, \mathbf{e}_3\}$ the *fixed inertial frame* in Euclidean space, and choose $\mathbf{e}_i = \delta_i^j \mathbf{E}_j$, where $\{\mathbf{E}_j\}$ is the *standard basis* in \mathbb{R}^3 . We then have the component expressions

$$\begin{aligned} \varphi &= \varphi^i \mathbf{e}_i, & \varphi_\alpha &= \varphi_{,\alpha}^i \mathbf{e}_i, & \delta\varphi &= \delta\varphi^i \mathbf{e}_i, \\ \mathbf{t} &= t^i \mathbf{e}_i, & \delta\mathbf{t} &= \delta t^i \mathbf{e}_i, & \Lambda &= \Lambda^i_j \mathbf{e}_i \otimes \mathbf{E}^j. \end{aligned} \quad (2.11)$$

²Throughout this presentation, unless otherwise stated, Greek indices range only over {1, 2}; $\alpha, \beta, \delta, \gamma, \rho, \dots \in \{1, 2\}$.

Here, $\Lambda : \mathcal{A} \rightarrow \text{SO}(3)$ is the orthogonal matrix that maps a pre-selected vector of the standard basis into the director field; for instance, $t = \Lambda E_3$.

2.2. The strain fields on the mid-surfaces \mathcal{S}^0 and \mathcal{S}

The formulation of constitutive models in stress resultants requires a careful definition of the strain measures associated with the current and reference placements of the shell. To make matters precise we define the following two linear spaces (see Fig. 2):

- (i) *Tangent plane to S at a point $\bar{x} \in \mathcal{S}$.* This is a two-dimensional subspace, denoted by $T_{\bar{x}}\mathcal{S}$, and given by

$$T_{\bar{x}}\mathcal{S} := \{h(\bar{x}) \mid h \cdot \varphi_{,1} \times \varphi_{,2} = 0\}. \quad (2.12)$$

An analogous definition holds for $T_{\bar{x}^0}\mathcal{S}^0$.

- (ii) *Tangent space at a point $\bar{x} \in \mathcal{S}$.* This is a three-dimensional space, isomorphic to \mathbb{R}^3 and denoted by $\mathcal{V}_{\bar{x}}$, which is given by

$$\mathcal{V}_{\bar{x}} := \{v = \alpha h + \beta t \mid h \in T_{\bar{x}}\mathcal{S} \text{ and } \alpha, \beta \in \mathbb{R}\}. \quad (2.13)$$

An identical definition holds for $\mathcal{V}_{\bar{x}^0}$.

With these definitions in hand, we consider the following *surface tensors*.

- (iii) *(Surface) deformation gradient.* A two-point tensor $\bar{F} : \mathcal{V}_{x^0} \rightarrow \mathcal{V}_x$ (for each $x^0 \in \mathcal{S}^0$) given by

$$\bar{F} = a_\alpha \otimes a^{0\alpha} + t \otimes a^{0^3}. \quad (2.14)$$

- (iv) *(Surface) unit tensor on \mathcal{S} .* A bilinear form $1 : \mathcal{V}_x \times \mathcal{V}_x \rightarrow \mathbb{R}$ with associated covariant rank-two tensor given by

$$1 := a_{\alpha\beta} a^\alpha \otimes a^\beta + \gamma_\alpha (a^\alpha \otimes a^3 + a^3 \otimes a^\alpha) + a^3 \otimes a^3. \quad (2.15)$$

- (v) *Director curvature tensor on \mathcal{S} .* A bilinear form $\kappa : \mathcal{V}_x \times \mathcal{V}_x \rightarrow \mathbb{R}$ with associated covariant rank-two tensor given by

$$\kappa = \kappa_{\alpha\beta} a^\alpha \otimes a^\beta; \quad \kappa_{\alpha\beta} := \frac{1}{2} (t_{,\alpha} \cdot a_\beta + t_{,\beta} \cdot a_\alpha). \quad (2.16)$$

Identical definitions hold for the corresponding tensor fields defined on \mathcal{S}^0 and denoted

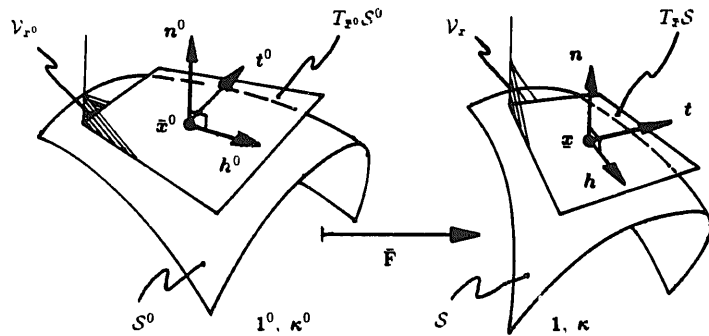


Fig. 2. Tangent planes and tangent spaces on the current and reference configurations.

defined as follows:

- (i) *Material rate-of-deformation tensors on \mathcal{S}^0* , are the time derivative of the corresponding strain tensors; i.e.,

$$\bar{\mathbf{D}}_\varphi := \dot{\bar{\mathbf{E}}}_\varphi \quad \text{and} \quad \bar{\mathbf{D}}_t := \dot{\bar{\mathbf{E}}}_t. \quad (2.22a)$$

In component form, in view of relations (2.14), definition (2.18) yields

$$\begin{aligned} \bar{\mathbf{D}}_\varphi &= \frac{1}{2}\dot{\mathbf{a}}_{\alpha\beta}\mathbf{a}^{0\alpha}\otimes\mathbf{a}^{0\beta} + \frac{1}{2}\dot{\gamma}^\alpha(\mathbf{a}^{0\alpha}\otimes\mathbf{a}^{03} + \mathbf{a}^{03}\otimes\mathbf{a}^{0\alpha}), \\ \bar{\mathbf{D}}_t &= \dot{\kappa}_{\alpha\beta}\mathbf{a}^{0\alpha}\otimes\mathbf{a}^{0\beta}. \end{aligned} \quad (2.22b)$$

- (ii) *Spatial rate-of-deformation tensors on \mathcal{S}* , are defined as the Lie derivatives of the spatial strain tensors on \mathcal{S} . Accordingly, we have

$$\begin{aligned} \bar{\mathbf{d}}_\varphi &:= L_v\bar{\mathbf{e}}_\varphi = \bar{\mathbf{F}}^{-1}\left[\frac{\partial}{\partial t}(\bar{\mathbf{F}}^t\bar{\mathbf{e}}_\varphi\bar{\mathbf{F}})\right]\bar{\mathbf{F}}^{-1}, \\ \bar{\mathbf{d}}_t &:= L_v\bar{\mathbf{e}}_t = \bar{\mathbf{F}}^{-1}\left[\frac{\partial}{\partial t}(\bar{\mathbf{F}}^t\bar{\mathbf{e}}_t\bar{\mathbf{F}})\right]\bar{\mathbf{F}}^{-1}. \end{aligned} \quad (2.23)$$

From (2.18) and (2.19), and noting that

$$\mathbf{a}^\alpha = \bar{\mathbf{F}}^{-1}\mathbf{a}^{0\alpha} \quad \text{and} \quad \mathbf{a}^3 = \bar{\mathbf{F}}^{-1}\mathbf{a}^{03}, \quad (2.24)$$

in components relative to the basis $\{\mathbf{a}^1, \mathbf{a}^2, \mathbf{a}^3\}$, we have

$$\begin{aligned} \bar{\mathbf{d}}_t &= \bar{\mathbf{F}}^{-1}[\dot{\bar{\mathbf{E}}}_\varphi]\bar{\mathbf{F}}^{-1} \\ &= \bar{\mathbf{F}}^{-1}[\dot{\kappa}_{\alpha\beta}\mathbf{a}^{0\alpha}\otimes\mathbf{a}^{0\beta}]\bar{\mathbf{F}}^{-1} \\ &= \dot{\kappa}_{\alpha\beta}(\bar{\mathbf{F}}^{-1}\mathbf{a}^{0\alpha})\otimes(\bar{\mathbf{F}}^{-1}\mathbf{a}^{0\beta}), \end{aligned} \quad (2.25)$$

and a similar expression for $\bar{\mathbf{d}}_\varphi$. Consequently, in view of (2.24), we conclude that

$$\begin{aligned} \bar{\mathbf{d}}_\varphi &= \frac{1}{2}\dot{\mathbf{a}}_{\alpha\beta}\mathbf{a}^\alpha\otimes\mathbf{a}^\beta + \frac{1}{2}\dot{\gamma}^\alpha(\mathbf{a}^\alpha\otimes\mathbf{a}^3 + \mathbf{a}^3\otimes\mathbf{a}^\alpha) \\ &= \dot{\mathbf{e}}_{\alpha\beta}\mathbf{a}^\alpha\otimes\mathbf{a}^\beta + \frac{1}{2}\dot{\delta}^\alpha(\mathbf{a}^\alpha\otimes\mathbf{a}^3 + \mathbf{a}^3\otimes\mathbf{a}^\alpha), \\ \bar{\mathbf{d}}_t &= \dot{\kappa}_{\alpha\beta}\mathbf{a}^\alpha\otimes\mathbf{a}^\beta = \dot{\rho}_{\alpha\beta}\mathbf{a}^\alpha\otimes\mathbf{a}^\beta. \end{aligned} \quad (2.26)$$

Again, we observe that the components of the spatial rates of deformation tensors $\bar{\mathbf{d}}_\varphi$ and $\bar{\mathbf{d}}_t$ on \mathcal{S} relative to $\{\mathbf{a}_1, \mathbf{a}_2, \mathbf{t}\}$ are identical to the components of the material rate-of-deformation tensors $\bar{\mathbf{D}}_\varphi$ and $\bar{\mathbf{D}}_t$ on \mathcal{S}^0 relative to the basis $\{\mathbf{a}_1^0, \mathbf{a}_2^0, \mathbf{t}^0\}$.

2.4. Stress resultants and stress couples

With the kinematic quantities defined above in hand, we next introduce the stress resultants and stress couples defined in Part I.

- (i) *Stress resultants on \mathcal{S}* . The *effective stress resultants* and *stress couples* on the current

surface \mathcal{S} are denoted by³

$$\tilde{\mathbf{n}} = \tilde{n}^{\alpha\beta} \mathbf{a}_\alpha \otimes \mathbf{a}_\beta + \tilde{q}^\alpha (\mathbf{a}_\alpha \otimes \mathbf{t} + \mathbf{t} \otimes \mathbf{a}_\alpha), \quad \tilde{\mathbf{m}} = \tilde{m}^{\alpha\beta} \mathbf{a}_\alpha \otimes \mathbf{a}_\beta. \quad (2.27)$$

We recall that an important consequence of balance of angular momentum is the symmetry of the membrane effective resultants $\tilde{n}^{\alpha\beta}$. This property is also assumed to hold for $\tilde{m}^{\alpha\beta}$. Consequently, one has

$$\tilde{n}^{\alpha\beta} = \tilde{n}^{\beta\alpha} \quad \text{and} \quad \tilde{m}^{\alpha\beta} = \tilde{m}^{\beta\alpha}, \quad \alpha = 1, 2. \quad (2.28)$$

(ii) *Stress resultants on \mathcal{S}^0 .* As in Part III, the effective stress resultants and stress couples on the reference surface \mathcal{S}^0 are defined via pull-back operation with $\bar{F} : \mathcal{V}_{x_0} \rightarrow \mathcal{V}_x$ as

$$\tilde{N} := \bar{J} \bar{F}^{-1} \tilde{\mathbf{n}} \bar{F}^{-1} \quad \text{and} \quad \tilde{M} := \bar{J} \bar{F}^{-1} \tilde{\mathbf{m}} \bar{F}^{-1}. \quad (2.29)$$

Again by exploiting the fact that $\mathbf{a}_\alpha = \bar{F} \mathbf{a}_\alpha^0$, from (2.27) and (2.29) we conclude that, up to a factor of \bar{J} , the components of $\tilde{\mathbf{n}}$ and $\tilde{\mathbf{m}}$ relative to $\{\mathbf{a}_1, \mathbf{a}_2, \mathbf{t}\}$ are equal to the components of \tilde{N} and \tilde{M} relative to $\{\mathbf{a}_1^0, \mathbf{a}_2^0, \mathbf{t}^0\}$; for example,

$$\begin{aligned} \tilde{N} &= \bar{J} [\tilde{n}^{\alpha\beta} \mathbf{a}_\alpha^0 \otimes \mathbf{a}_\beta^0 + \tilde{q}^\alpha (\mathbf{a}_\alpha^0 \otimes \mathbf{t}^0 + \mathbf{t}^0 \otimes \mathbf{a}_\alpha^0)], \\ \tilde{M} &= \bar{J} \tilde{m}^{\alpha\beta} \mathbf{a}_\alpha^0 \otimes \mathbf{a}_\beta^0. \end{aligned} \quad (2.30)$$

It can easily be shown that the stress power expression takes the following form:

$$\begin{aligned} \mathcal{W} &= \int_{\mathcal{S}} [\tilde{\mathbf{n}} : \bar{\mathbf{d}}_\varphi + \tilde{\mathbf{m}} : \bar{\mathbf{d}}_t] \bar{J} d\mu^0 \\ &= \int_{\mathcal{S}} [\tilde{N} : \bar{\mathbf{D}}_\varphi + \tilde{M} : \bar{\mathbf{D}}_t] d\mu^0 \\ &= \int_{\mathcal{S}} [\tilde{n}^{\alpha\beta} \frac{1}{2} \dot{a}_{\alpha\beta} + \tilde{q}^\alpha \dot{\gamma}_\alpha + \tilde{m}^{\alpha\beta} \dot{\kappa}_{\alpha\beta}] \bar{J} d\mu^0, \end{aligned} \quad (2.31)$$

where $d\mu^0 := \bar{j}^0 d\xi^1 d\xi^2$.

2.5. Matrix formulation: summary of notation

It should be clear from the preceding discussion that the only relevant objects in the definition of the state of stress and deformation of the shell are the tensor components $\{\tilde{n}^{\alpha\beta}, \tilde{q}^\alpha, \tilde{m}^{\alpha\beta}\}$ and $\{\mathbf{a}_{\alpha\beta}, \gamma_\alpha, \kappa_{\alpha\beta}\}$. These objects can be interpreted as components of tensors either on the reference surface \mathcal{S}^0 , or on the current surface \mathcal{S} , according to the definitions given above. It then proves convenient to introduce matrix notation and set

$$\mathbf{e}(\Phi) = \frac{1}{2} \begin{Bmatrix} a_{11} - a_{11}^0 \\ a_{22} - a_{22}^0 \\ 2(a_{12} - a_{12}^0) \end{Bmatrix}, \quad \boldsymbol{\delta}(\Phi) = \begin{Bmatrix} \gamma_1 - \gamma_1^0 \\ \gamma_2 - \gamma_2^0 \end{Bmatrix}, \quad \boldsymbol{\rho}(\Phi) = \begin{Bmatrix} \kappa_{11} - \kappa_{11}^0 \\ \kappa_{22} - \kappa_{22}^0 \\ 2(\kappa_{12} - \kappa_{12}^0) \end{Bmatrix}, \quad (2.32)$$

³ This is at variance with Parts I and III in which \tilde{q}^α , $\alpha \in \{1, 2\}$, are not included in $\tilde{\mathbf{n}}$, but rather are treated separately.

along with

$$\mathbf{n} = \bar{J} \begin{Bmatrix} \tilde{n}^{11} \\ \tilde{n}^{22} \\ \tilde{n}^{12} \end{Bmatrix}, \quad \mathbf{q} = \bar{J} \begin{Bmatrix} \tilde{q}^1 \\ \tilde{q}^2 \end{Bmatrix}, \quad \mathbf{m} = \bar{J} \begin{Bmatrix} \tilde{m}^{11} \\ \tilde{m}^{22} \\ \tilde{m}^{12} \end{Bmatrix}. \quad (2.33)$$

Furthermore, for convenience we also set

$$\boldsymbol{\sigma} = \begin{Bmatrix} \mathbf{n} \\ \mathbf{q} \\ \mathbf{m} \end{Bmatrix}, \quad \boldsymbol{\varepsilon}(\Phi) = \begin{Bmatrix} \boldsymbol{\epsilon}(\Phi) \\ \boldsymbol{\delta}(\Phi) \\ \boldsymbol{\rho}(\Phi) \end{Bmatrix}, \quad \dot{\boldsymbol{\varepsilon}}(\Phi) = \begin{Bmatrix} \dot{\boldsymbol{\epsilon}}(\Phi) \\ \dot{\boldsymbol{\delta}}(\Phi) \\ \dot{\boldsymbol{\rho}}(\Phi) \end{Bmatrix}, \quad (2.34)$$

where $\boldsymbol{\sigma}$, with \bar{J} scaling the *Cauchy* stress resultants, is interpreted as components of *Kirchhoff* stress resultants. The rate-of-deformation $\dot{\boldsymbol{\varepsilon}}(\Phi)$ is related to the velocity field through the matrix expression

$$\dot{\boldsymbol{\varepsilon}}(\Phi) = \mathbb{B}(\Phi) \begin{Bmatrix} \dot{\boldsymbol{\varphi}} \\ \dot{\mathbf{T}} \end{Bmatrix}, \quad \mathbb{B}(\Phi) = \begin{bmatrix} \mathbb{B}_m & \mathbb{0} \\ \mathbb{B}_{sm} & \mathbb{B}_{sb} \\ \mathbb{B}_{bm} & \mathbb{B}_{bb} \end{bmatrix}, \quad (2.35)$$

where we have used the notation summarized in Box 1 of Part III. The weak form of the equations of equilibrium then takes the form (see Parts I and III)

$$G(\boldsymbol{\sigma}, \Phi; \delta\Phi) := \int_{\omega} \mathbb{B}(\Phi) \left\{ \frac{\delta\boldsymbol{\varphi}}{\delta T} \right\} \cdot \boldsymbol{\sigma} d\mu^0 - \mathcal{G}_{\text{ext}}(\delta\Phi) = 0, \quad (2.36)$$

for all admissible variations $\delta\Phi = (\delta\boldsymbol{\varphi}, \delta\mathbf{T}) \in T_{\Phi}\mathcal{C}$, where $T_{\Phi}\mathcal{C}$ is the tangent space of variations defined in Part I. Recall that $\delta\mathbf{T} = \bar{\Lambda} \delta T$ where $\bar{\Lambda}$ is a 3×2 submatrix of the orthogonal matrix Λ mapping a vector $\mathbf{E} \in S^2$ into the current director \mathbf{T} , as explained in detail in Part III. As usual, $\mathcal{G}_{\text{ext}}(\delta\Phi)$ is the weak form of the external loading given by (2.32) of Part III.

Finally, for later reference, we record a form of the linearized *discrete* weak form which is valid for elastic or elastoplastic constitutive equations. Recall that linearization of the discrete weak form, following the notation of Section 5 in Part III, is split into geometric and material parts as

$$DG(\Phi_{n+1}; \delta\Phi) \cdot \Delta\Phi_{n+1} = DG_G(\Phi_{n+1}; \delta\Phi) \cdot \Delta\Phi_{n+1} + DG_M(\Phi_{n+1}; \delta\Phi) \cdot \Delta\Phi_{n+1}. \quad (2.37)$$

In the case of elastoplasticity, the *geometric* part $DG_G(\Phi_{n+1}; \delta\Phi) \cdot \Delta\Phi_{n+1}$ takes exactly the same form as in the purely elastic case discussed in Section 5 of Part III, except the stress resultants $\{\mathbf{n}, \mathbf{q}, \mathbf{m}\}$ are now evaluated simply using the discrete elastoplastic constitutive discussed below. The *material* part, $DG_M(\Phi_{n+1}; \delta\Phi) \cdot \Delta\Phi_{n+1}$, on the other hand, takes a somewhat different form, which for now will be represented in the form

$$D_M G(\Phi_{n+1}; \delta\Phi) \cdot \Delta\Phi_{n+1} = \int_{\omega} \left\{ \frac{\delta\boldsymbol{\varphi}}{\delta T} \right\}^t \mathbb{B}^t \left[\frac{d\boldsymbol{\sigma}_{n+1}}{d\boldsymbol{\varepsilon}_{n+1}} \right] \mathbb{B} \left\{ \frac{\Delta\boldsymbol{\varphi}_{n+1}}{\Delta T_{n+1}} \right\} d\mu^0. \quad (2.38)$$

Once $d\boldsymbol{\sigma}_{n+1}/d\boldsymbol{\varepsilon}_{n+1}$ is specified in (2.38), $DG(\Phi^k; \delta\Phi) \cdot \Delta\Phi^k$ becomes completely defined. We refer to $d\boldsymbol{\sigma}_{n+1}/d\boldsymbol{\varepsilon}_{n+1}$ as the *consistent algorithmic tangent moduli*.

3. Structure of the elastoplastic constitutive model

In this section, we outline the structure of the elastoplastic constitutive model considered in this paper. First, we consider the formulation of the model in ‘intrinsic’ form in terms of the kinematic quantities defined in the preceding section. Subsequently, we revert to matrix notation and show that for implementational purposes, the structure of the model is identical to that of the linearized theory. For further information on elastoplasticity at finite strains, we refer to the monograph of Simo and Hughes [2].

3.1. Plastic strain and plastic rate of deformation tensor

To characterize plastic flow, we introduce spatial strain tensors defined on \mathcal{S} , denoted by $\bar{\mathbf{e}}_\varphi^p$ and $\bar{\mathbf{e}}_t^p$, with components (cf. (2.18a))

$$\begin{aligned}\bar{\mathbf{e}}_\varphi^p &= e_{\alpha\beta}^p \mathbf{a}^\alpha \otimes \mathbf{a}^\beta + \frac{1}{2} \delta_\alpha^p (\mathbf{a}^\alpha \otimes \mathbf{a}^3 + \mathbf{a}^3 \otimes \mathbf{a}^\alpha), \\ \bar{\mathbf{e}}_t^p &= \rho_{\alpha\beta}^p \mathbf{a}^\alpha \otimes \mathbf{a}^\beta.\end{aligned}\quad (3.1)$$

Note that by pull-back with $\bar{\mathbf{F}} : \mathcal{V}_{x_0} \rightarrow \mathcal{V}_x$ we obtain plastic strain tensors on \mathcal{V}_{x_0} , denoted by $\bar{\mathbf{E}}_\varphi^p$ and $\bar{\mathbf{E}}_t^p$, respectively, and given by

$$\begin{aligned}\bar{\mathbf{E}}_\varphi^p &= e_{\alpha\beta}^p \mathbf{a}^{0\alpha} \otimes \mathbf{a}^{0\beta} + \frac{1}{2} \delta_\alpha^p (\mathbf{a}^{0\alpha} \otimes \mathbf{a}^{03} + \mathbf{a}^{03} \otimes \mathbf{a}^{0\alpha}), \\ \bar{\mathbf{E}}_t^p &= \rho_{\alpha\beta}^p \mathbf{a}^{0\alpha} \otimes \mathbf{a}^{0\beta}.\end{aligned}\quad (3.2)$$

Rates of deformation tensors are defined exactly as in the preceding section; i.e.,

$$\begin{aligned}\bar{\mathbf{d}}_\varphi^p &= L_v \bar{\mathbf{e}}_\varphi^p \quad \text{and} \quad \bar{\mathbf{d}}_t^p = L_v \bar{\mathbf{e}}_t^p, \\ \bar{\mathbf{D}}_\varphi^p &= \dot{\bar{\mathbf{E}}}_\varphi^p \quad \text{and} \quad \bar{\mathbf{D}}_t^p = \dot{\bar{\mathbf{E}}}_t^p.\end{aligned}\quad (3.3)$$

Again we observe that the components of $\{\bar{\mathbf{d}}_\varphi^p, \bar{\mathbf{d}}_t^p\}$ and $\{\bar{\mathbf{D}}_\varphi^p, \bar{\mathbf{D}}_t^p\}$ relative to the basis $\{\mathbf{a}_\alpha, t\}$ and $\{\mathbf{a}_\alpha^0, t^0\}$, respectively, coincide. For instance, we have (cf. (2.26))

$$\begin{aligned}\bar{\mathbf{d}}_\varphi^p &= e_{\alpha\beta}^p \mathbf{a}^\alpha \otimes \mathbf{a}^\beta + \frac{1}{2} \dot{\delta}_\alpha^p (\mathbf{a}^\alpha \otimes \mathbf{a}^3 + \mathbf{a}^3 \otimes \mathbf{a}^\alpha), \\ \bar{\mathbf{d}}_t^p &= \dot{\rho}_{\alpha\beta}^p \mathbf{a}^\alpha \otimes \mathbf{a}^\beta.\end{aligned}\quad (3.4)$$

This conclusion is the result of using convected coordinates.

3.2. Hyperelastic stress response

We characterize the stress response by means of a free energy function of the form

$$W = \hat{W}(\bar{\mathbf{e}}_\varphi, \bar{\mathbf{e}}_t; \bar{\mathbf{e}}_\varphi^p, \bar{\mathbf{e}}_t^p; \bar{\mathbf{F}}, \mathbf{1}^0). \quad (3.5)$$

Frame indifference (or covariance) requires that W depend on the strains and $\bar{\mathbf{F}}$ through the pull-backs of the strains with $\bar{\mathbf{F}}$; i.e.,

$$W = \bar{W}(\bar{\mathbf{E}}_\varphi, \bar{\mathbf{E}}_t; \bar{\mathbf{E}}_\varphi^p, \bar{\mathbf{E}}_t^p, \mathbf{1}^0). \quad (3.6)$$

In components we simply have

$$W = \bar{W}(e_{\alpha\beta}, \delta_\alpha, \rho_{\alpha\beta}, e_{\alpha\beta}^p, \delta_{\alpha\beta}^p, \rho_{\alpha\beta}^p, \mathbf{1}^0). \quad (3.7)$$

As in expressions (3.5) and (3.6), the dependence of \bar{W} in (3.7) on the reference metric $\mathbf{1}^0$ is understood.

Standard arguments then lead to the constitutive equations

$$\bar{J}\tilde{n}^{\alpha\beta} = \frac{\partial \bar{W}}{\partial e_{\alpha\beta}}, \quad \bar{J}\tilde{q}^\alpha = \frac{\partial \bar{W}}{\partial \delta_\alpha}, \quad \bar{J}\tilde{m}^{\alpha\beta} = \frac{\partial \bar{W}}{\partial \rho_{\alpha\beta}}. \quad (3.8)$$

In our numerical implementation, for reasons of simplicity, we restrict our attention to the following simple constitutive equation:

$$\begin{aligned} \bar{J}\tilde{n}^{\alpha\beta} &= \frac{Eh}{1-\nu^2} H^{\alpha\beta\gamma\eta} (e_{\gamma\eta} - e_{\gamma\eta}^p), \\ \bar{J}\tilde{q}^\alpha &= Gh\kappa a^{0\alpha\beta} (\delta_\beta - \delta_\beta^p), \\ \bar{J}\tilde{m}^{\alpha\beta} &= \frac{Eh^3}{12(1-\nu^2)} H^{\alpha\beta\gamma\eta} (\rho_{\gamma\eta} - \rho_{\gamma\eta}^p), \end{aligned} \quad (3.9)$$

where $h := h_+ - h_-$ is the thickness of the shell, $E > 0$ and $G > 0$ are interpreted as elastic moduli, and $\nu \in [0, \frac{1}{2}]$ as Poisson's ratio, and $H^{\alpha\beta\gamma\delta}$ is given by

$$H^{\alpha\beta\gamma\delta} := \nu a^{0\alpha\beta} a^{0\gamma\delta} + \frac{1}{2}(1-\nu)[a^{0\alpha\gamma} a^{0\beta\delta} + a^{0\beta\gamma} a^{0\alpha\delta}]. \quad (3.10)$$

In (3.9), the rate of deformation tensors \bar{d}_φ and \bar{d}_t are assumed to *additively decompose* into elastic and plastic parts, denoted $\{\bar{d}_\varphi^e, \bar{d}_\varphi^p\}$ and $\{\bar{d}_t^e, \bar{d}_t^p\}$, respectively; i.e.,

$$\begin{aligned} \bar{d}_\varphi &= \bar{d}_\varphi^e + \bar{d}_\varphi^p, \\ \bar{d}_t &= \bar{d}_t^e + \bar{d}_t^p. \end{aligned} \quad (3.11)$$

Consequently, from (2.26) and (3.4) the strain measures, using the matrix notation $\boldsymbol{\varepsilon} \in \mathbb{R}^8$ of (2.34), additively decompose into elastic and plastic parts, denoted by $\boldsymbol{\varepsilon}^e \in \mathbb{R}^8$ and $\boldsymbol{\varepsilon}^p \in \mathbb{R}^8$, respectively; i.e., $\boldsymbol{\varepsilon} = \boldsymbol{\varepsilon}^e + \boldsymbol{\varepsilon}^p$.

3.3. Yield condition, flow rule and hardening law

Conceptually, one characterizes the plastic response by means of a yield function formulated in stress space of the form

$$\phi = \bar{\phi}(\bar{J}\tilde{n}^{\alpha\beta}, \bar{J}\tilde{q}^\alpha, \bar{J}\tilde{m}^{\alpha\beta}; p^s, \mathbf{1}^0), \quad (3.12)$$

where p^s , $s = 1, \dots, m$, are the components of m internal variables characterizing the hardening response of the material. We assume an associative flow rule of the form

$$\begin{aligned}\dot{\epsilon}_{\alpha\beta}^p &= \dot{\gamma} \frac{1}{\bar{J}} \frac{\partial \bar{\phi}}{\partial \tilde{n}^{\alpha\beta}}, \\ \dot{\delta}_\alpha^p &= \dot{\gamma} \frac{1}{\bar{J}} \frac{\partial \bar{\phi}}{\partial \tilde{q}^\alpha}, \\ \dot{\rho}_{\alpha\beta}^p &= \dot{\gamma} \frac{1}{\bar{J}} \frac{\partial \bar{\phi}}{\partial \tilde{m}^{\alpha\beta}},\end{aligned}\tag{3.13}$$

and a general hardening law given in terms of generalized hardening moduli $h^s(\bar{J}\tilde{n}^{\alpha\beta}, \bar{J}\tilde{q}^\alpha, \bar{J}\tilde{m}^{\alpha\beta}; p^s)$ as

$$\dot{p}^s = \dot{\gamma} h^s(\bar{J}\tilde{n}^{\alpha\beta}, \bar{J}\tilde{q}^\alpha, \bar{J}\tilde{m}^{\alpha\beta}; p^s, \mathbf{1}^0), \quad s = 1, 2, \dots, m. \tag{3.14}$$

Notice that the yield function (3.12) and the flow rule (3.13) are formulated in terms of the Kirchhoff stress resultants, consistent with (3.8). In these evolution equations, $\dot{\gamma} \geq 0$ is the plastic consistency parameter; a function satisfying the Kuhn–Tucker complementary conditions

$$\dot{\gamma} \geq 0, \quad \bar{\phi} \leq 0, \quad \dot{\gamma}\bar{\phi} = \dot{\gamma}\hat{\phi} = 0, \tag{3.15}$$

which complete the formulation of the plasticity model.

REMARKS 3.1. (1) In view of relations (2.27) and (2.30), the yield condition (3.12) may be interpreted either as a function depending on the spatial quantities \tilde{n} , \tilde{m} , the deformation gradient \bar{F} (and the reference metric tensor $\mathbf{1}^0$) as

$$\phi = \hat{\phi}(\bar{J}\tilde{n}, \bar{J}\tilde{m}; p^s, \bar{F}, \mathbf{1}^0), \tag{3.16}$$

or as a function of \tilde{N} , \tilde{M} according to the pull-back relations

$$\begin{aligned}\bar{\phi} &= \tilde{\phi}(\bar{J}\bar{F}^{-1}\tilde{n}\bar{F}^{-1}, \bar{J}\bar{F}^{-1}\tilde{m}\bar{F}^{-1}, p^s, \mathbf{1}^0) \\ &= \tilde{\phi}(\tilde{N}, \tilde{M}, p^s, \mathbf{1}^0).\end{aligned}\tag{3.17}$$

However, when use is made of convected coordinates, the coordinate expression of ϕ reduces, in (3.16) and (3.17), to (3.12).

(2) Similarly, the flow equations (3.13) can be interpreted in the spatial description, as defining evolution equations of the form

$$\bar{d}_\varphi^p = \dot{\gamma} \frac{1}{\bar{J}} \frac{\partial \bar{\phi}}{\partial \tilde{n}} \quad \text{and} \quad \bar{d}_t^p = \dot{\gamma} \frac{1}{\bar{J}} \frac{\partial \bar{\phi}}{\partial \tilde{m}}; \tag{3.18a}$$

or, equivalently, in the material description as defining evolution equations of the form

$$\dot{\bar{E}}_\varphi^p = \dot{\gamma} \frac{\partial \tilde{\phi}}{\partial \tilde{N}} \quad \text{and} \quad \dot{\bar{E}}_t^p = \dot{\gamma} \frac{\partial \tilde{\phi}}{\partial \tilde{M}}; \tag{3.18b}$$

the equivalence of both descriptions is again the result of using convective coordinates.

(3) In the formulation of (3.12) and (3.18) we have assumed for simplicity that the function ϕ is smooth. Such an assumption is not realistic for models formulated in terms of stress resultants, where ϕ is typically non-smooth. This situation is considered in detail in Section 4 following the general development presented by Simo et al. [9].

4. Continuum elastoplastic model in stress resultants

In this section we summarize a general framework which encompasses a broad class of resultant based elastoplastic constitutive models suitable for shells. Many common elastoplastic models for resultant based shells fit into this framework (see [4–8] and the review article by Robinson [14]). In addition, we focus on a specific model based on a generalization of the two-surface yield criterion proposed by Shapiro [7]. Throughout this development, the stress measures $\{n, q, m\}$ and strain measures $\{e, \delta, \rho\}$ are assumed to be expressed in the *local Cartesian frame*, as defined in Section 3.1. of Part II.

4.1. General multisurface elastoplastic model: basic equations

To aid in constructing the elastoplastic model, the matrix notation introduced in Section 2.5 for the stress resultants $\sigma \in \mathbb{R}^8$, strain measures $\epsilon \in \mathbb{R}^8$ and plastic strains $\epsilon^P \in \mathbb{R}^8$, is used, where the stress resultants $\{n, q, m\}$ and strain measures $\{e, \delta, \rho\}$ are hereafter assumed to be resolved in the *local Cartesian frame*.

Following Simo et al. [9, 10], the set of internal variables p^s , $s = 1, \dots, m$, introduced in Section 3, is supplemented by a conjugate set of internal variables α_s , $s = 1, \dots, m$, through the transformation

$$\dot{p} = -\nabla \mathcal{H}(\alpha) \equiv -D\alpha, \quad (4.1)$$

where the hardening potential $\mathcal{H}(\alpha) := \frac{1}{2}\alpha^T D\alpha$, with $D \in \mathbb{R}^{m \times m} \times \mathbb{R}^{m \times m}$ constant, is assumed to be strictly quadratic, for simplicity. The *hyperelastic stress response* (3.8), in matrix notation, then becomes

$$\sigma = \nabla W(\epsilon - \epsilon^P), \quad (4.2)$$

where, again, σ are the Kirchhoff stress resultant components (cf. (3.8)). The *dissipation function* \mathcal{D}^P , representing the energy dissipated in plastic processes, then takes the form

$$\mathcal{D}^P[\sigma, p; \dot{\epsilon}^P, \dot{\alpha}] := \sigma^T \dot{\epsilon}^P + p^T \dot{\alpha} \geq 0. \quad (4.3)$$

Relations (4.1)–(4.3) have a sound thermodynamic basis which is discussed briefly in Appendix B.

Motivated by the fact that yield criteria for *resultant based* shell models typically entail multiple yield functions, we consider the case in which the *elastic domain*, denoted by $E_\sigma \subset \mathbb{R}^8 \times \mathbb{R}^P$, and its boundary, denoted by ∂E_σ , are defined as

$$\begin{aligned} E_\sigma &:= \{(\sigma, p) \in \mathbb{R}^8 \times \mathbb{R}^P \mid \phi_\mu(\sigma, p) < 0, \quad \text{for all } \mu \in [1, 2, \dots, m]\}, \\ \partial E_\sigma &:= \{(\sigma, p) \in \mathbb{R}^8 \times \mathbb{R}^P \mid \phi_\mu(\sigma, p) = 0, \quad \text{for some } \mu \in [1, 2, \dots, m]\}, \end{aligned} \quad (4.4)$$

where $\phi_\mu(\sigma, p)$ are $m \geq 1$ *smooth* functions which are assumed to define *independent*

constraints at any $(\sigma, p) \in \partial E_\sigma$ ⁴ and may intersect in a non-smooth fashion. The closure $E_\sigma \cup \partial E_\sigma$ is assumed to be a closed convex set.

The evolution of the plastic strains $\dot{\epsilon}^p$ and the internal variables $\dot{\alpha}$ take the form

$$\begin{aligned}\dot{\epsilon}^p &= \sum_{\mu=1}^m \dot{\gamma}^\mu \partial_\sigma \phi_\mu(\sigma, p), \\ \dot{\alpha} &= \sum_{\mu=1}^m \dot{\gamma}^\mu \partial_p \phi_\mu(\sigma, p),\end{aligned}\tag{4.5a}$$

where, for simplicity, attention is restricted to the *associative* case. Here, $\dot{\omega}$ represents ordinary time differentiation of ω . Notice that so-called ‘objective rates’ are avoided in the *component* expressions (4.5a), which, in terms of the notation introduced in Section 3, take the equivalent forms

$$\begin{aligned}\bar{d}_\varphi^p &= \sum_{\mu=1}^m \dot{\gamma}^\mu \frac{1}{J} \partial_{\tilde{n}} \hat{\phi}_\mu, & \bar{d}_t^p &= \sum_{\mu=1}^m \dot{\gamma}^\mu \frac{1}{J} \partial_{\tilde{m}} \hat{\phi}_\mu, \\ L_v \dot{\alpha} &= \sum_{\mu=1}^m \dot{\gamma}^\mu \partial_p \hat{\phi}_\mu,\end{aligned}\tag{4.5b}$$

where $\{\dot{\alpha}, \dot{p}\}$ are resolved in $\{a^1, a^2, a^3\}$ and $\{a_1, a_2, t\}$, respectively, with components $\{\alpha, p\}$. Frame invariance is guaranteed in (4.5a) by the use of the Lie derivatives (4.5b) in convected coordinates. In (4.5), $\dot{\gamma}^\mu$ are $m \geq 1$ *plastic consistency parameters*, which satisfy the following *Kuhn–Tucker complementarity conditions* for $\mu = 1, 2, \dots, m$:

$$\dot{\gamma}^\mu \geq 0, \quad \phi_\mu(\sigma, p) \leq 0 \quad \text{and} \quad \dot{\gamma}^\mu \phi_\mu(\sigma, p) = 0, \tag{4.6}$$

along with the consistency requirement

$$\dot{\gamma}^\mu \dot{\phi}_\mu(\sigma, p) = 0.⁵ \tag{4.7}$$

Conditions (4.5a)₁ and (4.6) are essentially the multisurface plasticity counterpart of those in Koiter [6, eq. (2.19)], and have been employed by several authors, notably Maier [16] and Maier and Grierson [17]. The associative expressions (4.5a) evolve from the classical *principle of maximum plastic/dissipation* (see [10]).

The above framework may be immediately extended to viscoplasticity by means of a generalized Duvaut–Lions model as discussed in [9]. Note that viscoplastic models of the Perzyna type (e.g., [18]) are not meaningful in the presence of multiple yield surfaces intersecting in a nonsmooth fashion.

4.2. Generalized Ilyushin–Shapiro elastoplastic model

We now specialize the general framework above to a particular model based on a proposed generalization of the yield criterion proposed by Shapiro [7] to include hardening. This model is considered here not only as a good approximation of the Von Mises criterion for shells, but also as a representative model for a general class of multi-surface resultant based elastoplastic formulations for shells. For simplicity, the stored energy function W and the hardening

⁴ For example, if $p = 0$ and $\dim E_\sigma = 8$, then at most eight independent surfaces can intersect at one point.

⁵ The summation convention on repeated indices is not enforced in (4.6) or (4.7).

potential \mathcal{H} are assumed to be strictly quadratic; i.e.,

$$\begin{aligned} W(\boldsymbol{\varepsilon} - \boldsymbol{\varepsilon}^p) &:= \frac{1}{2}(\boldsymbol{\varepsilon} - \boldsymbol{\varepsilon}^p)^t \mathbb{C}(\boldsymbol{\varepsilon} - \boldsymbol{\varepsilon}^p), \\ \mathcal{H}(\boldsymbol{\alpha}) &:= \frac{1}{2} \boldsymbol{\alpha}^t \mathbf{D} \boldsymbol{\alpha}. \end{aligned} \quad (4.8)$$

Here, \mathbb{C} and \mathbf{D} are constant and are taken to be of the form

$$\begin{aligned} \mathbb{C} := \nabla^2 W(\boldsymbol{\varepsilon} - \boldsymbol{\varepsilon}^p) &= \begin{bmatrix} \partial_{ee}^2 \hat{W} & \mathbf{0} & \mathbf{0} \\ \mathbf{0} & \partial_{\gamma\gamma}^2 \hat{W} & \mathbf{0} \\ \mathbf{0} & \mathbf{0} & \partial_{\kappa\kappa}^2 \hat{W} \end{bmatrix} = \begin{bmatrix} \mathbb{C}_n & \mathbf{0} & \mathbf{0} \\ \mathbf{0} & \mathbb{C}_q & \mathbf{0} \\ \mathbf{0} & \mathbf{0} & \mathbb{C}_m \end{bmatrix}, \\ \mathbf{D} := \nabla^2 \mathcal{H}(\boldsymbol{\alpha}) &= \begin{bmatrix} \partial_{\alpha\alpha}^2 \hat{\mathcal{H}} & \mathbf{0} \\ \mathbf{0} & \partial_{\bar{\alpha}\bar{\alpha}}^2 \hat{\mathcal{H}} \end{bmatrix} =: \begin{bmatrix} D & \mathbf{0} \\ \mathbf{0} & \bar{\mathbf{D}} \end{bmatrix}, \end{aligned} \quad (4.9)$$

where $\hat{W}(\boldsymbol{\varepsilon} - \boldsymbol{\varepsilon}^p, \boldsymbol{\gamma} - \boldsymbol{\gamma}^p, \boldsymbol{\kappa} - \boldsymbol{\kappa}^p) := W(\boldsymbol{\varepsilon} - \boldsymbol{\varepsilon}^p)$, $\hat{\mathcal{H}}(\boldsymbol{\alpha}, \bar{\boldsymbol{\alpha}}) := \mathcal{H}(\boldsymbol{\alpha})$, and

$$\begin{aligned} D &:= \frac{\kappa_0}{\kappa'}, \\ \bar{\mathbf{D}} &:= \frac{2}{3} H' \mathbf{1}_8. \end{aligned} \quad (4.10)$$

The constants $\{\kappa_0, \kappa', H'\}$ are yield parameters (defined below). The hardening variables $\alpha \in \mathbb{R}$ and $\bar{\alpha} \in \mathbb{R}^8$ are those associated with so-called isotropic and kinematic hardening of the yield surface, respectively. The quadratic forms (4.8) imply linear elastic and linear hardening behavior. For *isotropic* elastic response, we have

$$\begin{aligned} \mathbb{C}_n &:= h \bar{\mathbb{C}}, \\ \mathbb{C}_q &:= G h \kappa_s \mathbf{1}_2, \\ \mathbb{C}_m &:= \frac{h^3}{12} \bar{\mathbb{C}}, \\ \mathbb{C} &:= \frac{E}{1 - \nu^2} \begin{bmatrix} 1 & \nu & 0 \\ \nu & 1 & 0 \\ 0 & 0 & \frac{1-\nu}{2} \end{bmatrix}, \end{aligned} \quad (4.11)$$

where E is Young's modulus, ν is Poisson's ratio, $G\kappa$ is the effective (transverse) shear modulus, h is the shell thickness, $\bar{\mathbb{C}}$ is the standard *plane stress* elasticity matrix, and $\mathbf{1}_n$ denotes the rank- n identity matrix. The stress resultants $\boldsymbol{\sigma} \in \mathbb{R}^8$ and hardening variables $\boldsymbol{p} \in \mathbb{R}^9$ (conjugate to $\boldsymbol{\varepsilon} - \boldsymbol{\varepsilon}^p$ and $\boldsymbol{\alpha}$, respectively), from (4.1) and (4.2) then become

$$\begin{aligned} \boldsymbol{\sigma} &:= \nabla W(\boldsymbol{\varepsilon} - \boldsymbol{\varepsilon}^p) = \mathbb{C}(\boldsymbol{\varepsilon} - \boldsymbol{\varepsilon}^p), \\ \boldsymbol{p} &:= \begin{bmatrix} p \\ \boldsymbol{p} \end{bmatrix} = -\nabla \mathcal{H}(\boldsymbol{\alpha}) = -\mathbf{D} \boldsymbol{\alpha} = -\begin{bmatrix} D \boldsymbol{\alpha} \\ \bar{\mathbf{D}} \bar{\boldsymbol{\alpha}} \end{bmatrix}. \end{aligned} \quad (4.12)$$

The generalization of the yield criterion introduced by Shapiro [7] proposed here in terms of

the Kirchhoff stress resultants σ takes the form

$$\phi_\mu(\sigma, p) \equiv \bar{\phi}_\mu(\sigma + \bar{p}, p) := f_\mu(\sigma + \bar{p}) - \frac{\kappa^2(p)}{\kappa_0^2} \leq 0, \quad \mu \in \{1, 2\}, \quad (4.13)$$

where

$$\begin{aligned} \kappa(p) &:= \kappa_0 + \kappa' p, \\ f_\mu(\sigma + \bar{p}) &:= (\sigma + \bar{p})^T \mathbf{A}_\mu(\sigma + \bar{p}), \\ \mathbf{A}_\mu &:= \begin{bmatrix} \frac{1}{n_0^2} \mathbf{P} & \mathbf{0} & \frac{\text{sign}(\mu)}{2\sqrt{3}n_0m_0} \mathbf{P} \\ \mathbf{0} & \frac{1}{q_0^2} \mathbf{I}_2 & \mathbf{0} \\ \frac{\text{sign}(\mu)}{2\sqrt{3}n_0m_0} \mathbf{P} & \mathbf{0} & \frac{1}{m_0^2} \mathbf{P} \end{bmatrix}, \\ \text{sign}(\mu) &:= \begin{cases} +1, & \text{if } \mu = 1, \\ -1, & \text{if } \mu = 2, \end{cases} \\ \mathbf{P} &:= \begin{bmatrix} 1 & -\frac{1}{2} & 0 \\ -\frac{1}{2} & 1 & 0 \\ 0 & 0 & 3 \end{bmatrix}, \end{aligned} \quad (4.14)$$

and n_0 , q_0 and m_0 are the yield parameters associated with membrane, transverse shear and bending responses, respectively. These yield parameters are typically related to the uniaxial yield parameter κ_0 through the relations $n_0 = [h]\kappa_0$, $m_0 = [h^2/4]\kappa_0$ and $q_0 = [h/\sqrt{3}]\kappa_0$. The parameters κ' and H' are the hardening moduli associated with (linear) isotropic and kinematic hardening, respectively. Note that \bar{p} is the *negative* of the so-called *back stress*. If $\kappa' = 0$ and $H' = 0$ (or, equivalently $p \equiv 0$ and $\bar{p} \equiv 0$), then the Ilyushin–Shapiro yield criterion [7] is recovered. Nonlinear isotropic and kinematic hardening can also be accommodated without difficulty for suitable choices of the functions $\kappa(p)$ and $H'(p)$.

The evolution equations (4.5) for the plastic strains $\dot{\epsilon}^p$ and hardening variables $\dot{\alpha}$ take the form

$$\begin{aligned} \dot{\epsilon}^p &= \sum_{\mu \in \{1, 2\}} \dot{\gamma}^\mu 2\mathbf{A}_\mu(\sigma + \bar{p}), \\ \dot{\alpha} = \left\{ \begin{array}{c} \dot{\alpha} \\ \dot{\bar{p}} \end{array} \right\} &= \sum_{\mu \in \{1, 2\}} \dot{\gamma}^\mu \left\{ \begin{array}{c} -2\kappa'\kappa(p) \\ \frac{\kappa_0^2}{2\mathbf{A}_\mu(\sigma + \bar{p})} \end{array} \right\}, \end{aligned} \quad (4.15)$$

which implies that $\dot{\bar{p}} = \dot{\epsilon}^p$. Finally, with $\dot{p} := -\mathbf{D}\dot{\alpha}$, it follows that

$$\dot{p} = \left\{ \begin{array}{c} \dot{p} \\ \dot{\bar{p}} \end{array} \right\} = \left\{ \begin{array}{c} \mathcal{D}^p \\ -\frac{2}{3}H'\dot{\epsilon}^p \end{array} \right\}, \quad (4.16a)$$

where \mathcal{D}^p is defined in (4.3). That is, (4.16a)₁ is a generalization of the notion of equivalent plastic work $W^p := \sigma : \dot{\epsilon}^p$ as an internal variable (e.g., see [19, 20] for a discussion of W^p), whereas (4.16a)₂ is an extension to the current model of the Prager–Ziegler kinematic hardening law for J_2 -flow theory. In tensor form, (4.16a)₂ is equivalent to

$$L_v \hat{\bar{p}} = -\frac{2}{3} H' \begin{Bmatrix} \bar{d}_\varphi^P \\ \bar{d}_t^P \end{Bmatrix}, \quad (4.16b)$$

where $\hat{\bar{p}}$ is resolved in the basis $\{a_1, a_2, t\}$ with components \bar{p} .

To gain insight into the nature of the isotropic hardening mechanism defined by (4.14)₁ and (4.16a)₁, we consider the case of simple uniaxial tension. In a uniaxial tension state, this isotropic hardening mechanism evolves linearly with the total strain magnitude, as in classical J_2 -flow models with linear isotropic hardening (for classical J_2 -flow models, see, e.g., [3]). This is shown explicitly in Fig. 3 in which an isotropically hardening specimen is loaded in uniaxial tension using both the shell model above and a classical (plane stress) J_2 -flow model. The isotropic hardening mechanism in the latter case is defined by

$$\begin{aligned} \phi(\boldsymbol{\sigma}, \bar{e}^P) &:= \|s\| - (\kappa_0 + \kappa' \bar{e}^P), \\ \dot{\bar{e}}^P &:= \sqrt{\frac{2}{3}} \|\dot{\boldsymbol{\epsilon}}^P\|, \quad s := \text{dev } \boldsymbol{\sigma}, \end{aligned} \quad (4.17)$$

where $\boldsymbol{\sigma}$ and $\boldsymbol{\epsilon}^P$ have their classical definitions in J_2 -flow theory. Both responses depicted in Fig. 3 correspond to $E = 10$, $\kappa_0 = 0.2$, and $\kappa' = 9.0$. This comparison is particularly useful since, for plane stress conditions, (4.13) reduces precisely to the classical plane stress Von Mises yield criterion (ignoring hardening). From Fig. 3, it is evident that the classical isotropic hardening variable \bar{e}^P leads to considerably more severe hardening than \mathcal{D}^P , that associated with the shell model here. One can, however, adjust the slope corresponding to the shell model in Fig. 3 via κ' in (4.14)₁ to replicate any degree of linear hardening present in the classical model. Similarly, the kinematic hardening mechanism (4.16a)₂ also evolves linearly.

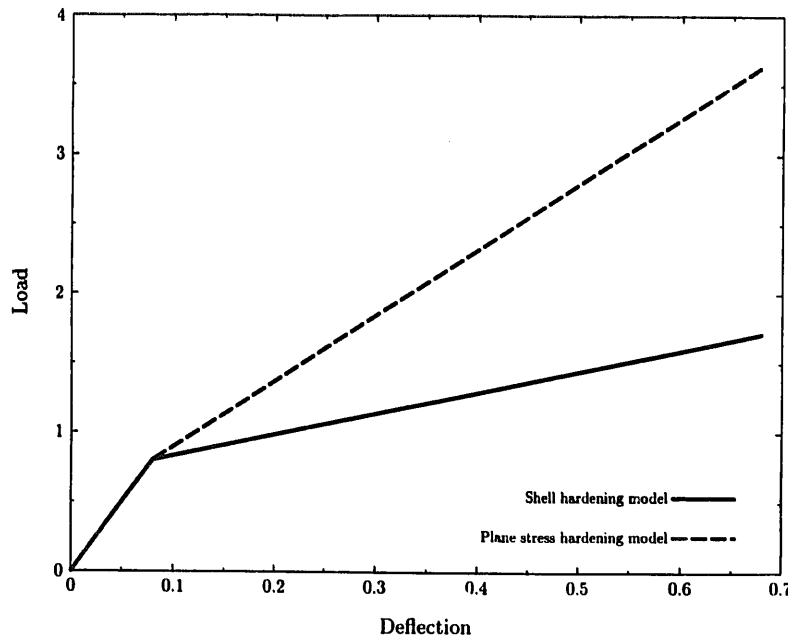


Fig. 3. Illustration of the linear isotropic hardening response for the proposed shell constitutive model. Comparison with the linear isotropic hardening response of classical J_2 -flow theory.

5. Elastoplastic return mapping algorithm: closest point projection

In this section we outline a general algorithm to integrate the continuum elastoplastic problem discussed in Section 4 on $t \in [0, T]$. The algorithm has the standard geometric interpretation of a closest-point-projection, in the energy norm, of a *trial state* onto the elastic domain. The crucial difference between the present multi-surface algorithm and standard single surface algorithms (see e.g. [2] for a review) concerns the determination of the active surfaces in the return mapping procedure.

5.1. Discrete algorithmic problem

Let $\bar{x} \in \mathcal{S}$ denote a *given* point on the current mid-surface of the shell. Consider a time discretization of the interval $[0, T] \subset \mathbb{R}$ of interest. The algorithmic problem addressed in this section is local in the sense that $\bar{x} \in \mathcal{S}$ is assumed fixed, but arbitrary. At $\bar{x} \in \mathcal{S}$ and time $t_n \in [0, T]$ we assume the state variables $\{\boldsymbol{\epsilon}_n, \boldsymbol{\epsilon}_n^p, \boldsymbol{\alpha}_n\}$ are known. Let $(\Delta\varphi_{n+1}, \Delta t_{n+1})$ be a *given* increment in the kinematic measures on the interval $t \in [t_n, t_{n+1}]$. The basic problem, then, is to update the fields $\{\boldsymbol{\epsilon}_n, \boldsymbol{\epsilon}_n^p, \boldsymbol{\alpha}_n\}$ at $t_n \in [0, T]$ to $\{\boldsymbol{\epsilon}_{n+1}, \boldsymbol{\epsilon}_{n+1}^p, \boldsymbol{\alpha}_{n+1}\}$ at $t_{n+1} \in [t_n, T]$ in a manner consistent with the continuum elastoplastic constitutive equations developed in Section 4. To this end, for the general model of Section 4.1, application of an implicit, backward Euler difference scheme to the evolution equations (4.5) leads to the following *nonlinear* coupled system for the state variables $\{\boldsymbol{\epsilon}_{n+1}, \boldsymbol{\epsilon}_{n+1}^p, \boldsymbol{\alpha}_{n+1}\}$ at time t_{n+1} :

$$\begin{aligned} \boldsymbol{\epsilon}_{n+1} &= \hat{\boldsymbol{\epsilon}}(\Delta\varphi_{n+1}, \Delta t_{n+1}) \quad (\text{given}), \\ \boldsymbol{\epsilon}_{n+1}^p &= \boldsymbol{\epsilon}_n^p + \sum_{\mu=1}^m \gamma_{n+1}^\mu \partial_{\boldsymbol{\sigma}} \phi_\mu(\boldsymbol{\sigma}, \bar{\boldsymbol{p}})_{n+1}, \\ \boldsymbol{\alpha}_{n+1} &= \boldsymbol{\alpha}_n + \sum_{\mu=1}^m \gamma_{n+1}^\mu \partial_{\boldsymbol{p}} \phi_\mu(\boldsymbol{\sigma}, \bar{\boldsymbol{p}})_{n+1}, \\ \boldsymbol{\sigma}_{n+1} &= \nabla W(\boldsymbol{\epsilon}_{n+1} - \boldsymbol{\epsilon}_{n+1}^p) = \mathbb{C}(\boldsymbol{\epsilon}_{n+1} - \boldsymbol{\epsilon}_{n+1}^p), \\ \boldsymbol{p}_{n+1} &= -\nabla \mathcal{H}(\boldsymbol{\alpha}_{n+1}) = -\mathbf{D}\boldsymbol{\alpha}_{n+1}, \end{aligned} \tag{5.1}$$

where we have set $\gamma_{n+1}^\mu := \Delta t \dot{\gamma}_{n+1}^\mu$, and $\hat{\boldsymbol{\epsilon}}(\Delta\varphi_{n+1}, \Delta t_{n+1})$ is the identical geometric update considered for the elastic case in Part III, regarded here simply as a given quantity in the return mapping algorithm. As noted previously, the use of convected coordinates precludes the need for ‘objective rates’ in the component forms of the evolution equations (4.5a). Consequently, so-called ‘incrementally objective’ algorithms of the type discussed by Hughes and Winget [21] to integrate such objective rates are not needed here. Incremental frame invariance of the algorithm is guaranteed by the use of the Lie derivative in convected coordinates. The discrete counterpart of the Kuhn–Tucker loading/unloading conditions (4.6) take the form

$$\gamma_{n+1}^\mu \geq 0, \quad \phi_\mu(\boldsymbol{\sigma}, \bar{\boldsymbol{p}})_{n+1} \leq 0 \quad \text{and} \quad \gamma_{n+1}^\mu \phi_\mu(\boldsymbol{\sigma}, \bar{\boldsymbol{p}})_{n+1} \equiv 0, \tag{5.2}$$

for $\mu = 1, 2$, but no sum on μ . By specializing the update algorithm (5.1) to the case of the current model in Section 4.2., (5.1)_{2,3} are replaced by

$$\begin{aligned}\boldsymbol{\varepsilon}_{n+1}^p &= \boldsymbol{\varepsilon}_n^p + \sum_{\mu \in \{1,2\}} \gamma_{n+1}^\mu 2\mathbf{A}_\mu(\boldsymbol{\sigma} + \bar{\boldsymbol{p}})_{n+1}, \\ \boldsymbol{\alpha}_{n+1} &= \left\{ \frac{\boldsymbol{\alpha}}{\bar{\boldsymbol{p}}} \right\}_{n+1} = \boldsymbol{\alpha}_n + \sum_{\mu \in \{1,2\}} \gamma_{n+1}^\mu \left\{ \begin{array}{l} \frac{-2\kappa' \kappa(p)}{\kappa_0^2} \\ 2\mathbf{A}_\mu(\boldsymbol{\sigma} + \bar{\boldsymbol{p}}) \end{array} \right\}_{n+1},\end{aligned}\quad (5.3)$$

whereas (5.1)_{1,4,5} remain unchanged. It follows that $\bar{\boldsymbol{\alpha}}_{n+1} = \boldsymbol{\varepsilon}_{n+1}^p$. The *elastic strain* measures $\boldsymbol{\varepsilon}^e$ and the *stress resultants* $\boldsymbol{\sigma}$ are regarded as *dependent* variables and are obtained through the hyperelastic stress-strain equations $\boldsymbol{\varepsilon}_{n+1}^e := \boldsymbol{\varepsilon}_{n+1} - \boldsymbol{\varepsilon}_{n+1}^p$ and $\boldsymbol{\sigma}_{n+1} = \nabla W(\boldsymbol{\varepsilon}_{n+1}^e)$.

The nonlinear system (5.1) (or (5.3)) subject to the unilateral constraints (5.2) defines the *discrete algorithmic problem*. Convexity of the admissible region $\mathbb{E}_\sigma \cup \partial\mathbb{E}_\sigma$ (which is guaranteed by a positive definite \mathbf{A}_μ , $\mu = 1, 2$, in (5.3)), renders this problem a *convex mathematical programming* problem with a unique solution. In particular, it is a convex minimization problem equivalent geometrically to the *closest-point-projection* of the trial state $\{\boldsymbol{\sigma}_{n+1}^{\text{trial}}, \boldsymbol{p}_{n+1}^{\text{trial}}\}$ onto the boundary of the elastic region $\partial\mathbb{E}_\sigma$ in the energy norm. The *trial state* is defined by ‘freezing the plastic flow’ in the interval $t \in [t_n, t_{n+1}]$. Accordingly, setting $\gamma_{n+1}^\mu = 0$, $\mu = 1, 2$, in (5.1) we obtain

$$\begin{aligned}\boldsymbol{\varepsilon}_{n+1}^{\text{trial}} &:= \boldsymbol{\varepsilon}_n^p, \\ \boldsymbol{\alpha}_{n+1}^{\text{trial}} &:= \boldsymbol{\alpha}_n, \\ \boldsymbol{\varepsilon}_{n+1}^e &:= \boldsymbol{\varepsilon}_{n+1} - \boldsymbol{\varepsilon}_n^p, \\ \boldsymbol{\sigma}_{n+1}^{\text{trial}} &:= \nabla W(\boldsymbol{\varepsilon}_{n+1}^e), \\ \boldsymbol{p}_{n+1}^{\text{trial}} &:= -\mathbf{D}\boldsymbol{\alpha}_{n+1}^{\text{trial}}, \\ \phi_{\mu,n+1}^{\text{trial}} &:= \phi_\mu(\boldsymbol{\sigma}_{n+1}^{\text{trial}}, \bar{\boldsymbol{p}}_{n+1}).\end{aligned}\quad (5.4)$$

The trial state arises naturally in the context of an *elastic-plastic operator split*.

5.2. Numerical solution strategy

The iterative solution algorithm for the general elastoplastic model in (5.1) is considered in [9]. Specialization of this iterative algorithm to the current model in (5.3), with combined isotropic/kinematic hardening, follows without fundamental difficulty. However, the particular form of ϕ_μ , $\mu \in \{1, 2\}$, in (4.13) allows for a significantly more efficient solution strategy. In particular, ϕ_μ , $\mu \in \{1, 2\}$, in (4.13) may be expressed exclusively in terms of the consistency parameters $\gamma_{n+1}^\mu \in \mathbb{R}$, $\mu \in \{1, 2\}$. Consequently, the return mapping reduces to the solution of the following nonlinear, rank-2 system:

$$\hat{\phi}_\mu(\gamma^1, \gamma^2)_{n+1} := \bar{\phi}_\mu(\boldsymbol{\sigma} + \bar{\boldsymbol{p}}, \boldsymbol{p})_{n+1} = 0, \quad \mu \in \{1, 2\}. \quad (5.5)$$

Although the explicit definition of the functional forms of $\hat{\phi}_\mu$, $\mu \in \{1, 2\}$, is a cumbersome and notationally intensive task, the development is conceptually straightforward, as is shown below.

5.2.1. Reduced rank-2 systems

The reduction (5.5) follows directly by expressing $\{\boldsymbol{\sigma} + \bar{\boldsymbol{p}}, \boldsymbol{p}\}_{n+1}$ exclusively in $\{\gamma^1, \gamma^2\}_{n+1}$.

Use of the elastic stress-strain equations $\boldsymbol{\sigma}_{n+1} = \mathbb{C}(\boldsymbol{\varepsilon}_{n+1} - \boldsymbol{\varepsilon}_{n+1}^p) \equiv \boldsymbol{\sigma}_{n+1}^{\text{trial}} - \mathbb{C}\Delta\boldsymbol{\varepsilon}_{n+1}^p$ along with (5.1)₅ and (5.3)₂ for \mathbf{p}_{n+1} yields

$$\left[\mathbf{1}_8 + \sum_{\mu \in \{1,2\}} \gamma_{n+1}^\mu \left(\frac{4}{3} H' \mathbf{A}_\mu + 2 \mathbb{C} \mathbf{A}_\mu \right) \right] \boldsymbol{\eta}_{n+1} = \boldsymbol{\eta}_{n+1}^{\text{trial}}, \quad (5.6)$$

where

$$\begin{aligned} \boldsymbol{\eta}_{n+1} &:= \begin{Bmatrix} \boldsymbol{\eta}_n \\ \boldsymbol{\eta}_q \\ \boldsymbol{\eta}_m \end{Bmatrix}_{n+1} := \begin{Bmatrix} \mathbf{n} + \bar{\mathbf{p}}_n \\ \mathbf{q} + \bar{\mathbf{p}}_q \\ \mathbf{m} + \bar{\mathbf{p}}_m \end{Bmatrix}_{n+1} \equiv \boldsymbol{\sigma}_{n+1} + \bar{\mathbf{p}}_{n+1}, \\ \bar{\mathbf{p}}_{n+1} &= : \begin{Bmatrix} \bar{\mathbf{p}}_n \\ \bar{\mathbf{p}}_q \\ \bar{\mathbf{p}}_m \end{Bmatrix}_{n+1}. \end{aligned} \quad (5.7)$$

Further, by noting that

$$\mathbb{C} \mathbf{A}_\mu = \begin{bmatrix} \frac{1}{n_0^2} \mathbb{C}_n \mathbf{P} & \mathbf{0} & \frac{\text{sign}(\mu)}{2\sqrt{3}n_0 m_0} \mathbb{C}_n \mathbf{P} \\ \mathbf{0} & \frac{1}{q_0^2} \mathbf{1}_2 & \mathbf{0} \\ \frac{\text{sign}(\mu)}{2\sqrt{3}n_0 m_0} \mathbb{C}_m \mathbf{P} & \mathbf{0} & \frac{1}{m_0^2} \mathbb{C}_m \mathbf{P} \end{bmatrix}, \quad (5.8)$$

we see that the linear system (5.6) is uncoupled in \mathbf{q}_{n+1} . In fact, from (5.6), we conclude that

$$\begin{aligned} \mathbf{q}_{n+1} &= \zeta(\gamma^1, \gamma^2)_{n+1} \mathbf{q}_{n+1}^{\text{trial}}, \\ \zeta(\gamma^1, \gamma^2)_{n+1} &:= \left(\frac{1}{1 + Gh\kappa \frac{2}{q_0^2} (\gamma^1 + \gamma^2)} \right)_{n+1}, \end{aligned} \quad (5.9)$$

where (4.11)₂ has been used for \mathbb{C}_q . For isotropic elastic response, the system (5.6) takes a remarkably simple form. In particular \mathbb{C}_n , \mathbb{C}_m and $\bar{\mathbb{C}}$ defined in (4.11), along with \mathbf{P} have the same characteristic subspaces. That is,

$$\mathbf{P} = \mathbf{Q} \Lambda_{\mathbf{P}} \mathbf{Q}^t, \quad \bar{\mathbb{C}} = \mathbf{Q} \Lambda_{\bar{\mathbb{C}}} \mathbf{Q}^t, \quad \mathbf{Q} := \frac{1}{\sqrt{2}} \begin{bmatrix} 1 & 1 & 0 \\ -1 & 1 & 0 \\ 0 & 0 & \sqrt{2} \end{bmatrix}, \quad (5.10)$$

where $\mathbf{Q}^{-1} = \mathbf{Q}^t$ is orthogonal and the diagonal matrices $\Lambda_{\mathbf{P}}$ and $\Lambda_{\bar{\mathbb{C}}}$ are given by

$$\Lambda_{\mathbf{P}} := \begin{bmatrix} \frac{1}{2} & 0 & 0 \\ 0 & \frac{3}{2} & 0 \\ 0 & 0 & 3 \end{bmatrix}, \quad \Lambda_{\bar{\mathbb{C}}} := \begin{bmatrix} \frac{E}{1-\nu} & 0 & 0 \\ 0 & \frac{E}{1+\nu} & 0 \\ 0 & 0 & \frac{E}{2(1+\nu)} \end{bmatrix}. \quad (5.11)$$

It follows that \mathbf{P} and $\bar{\mathbb{C}}$ commute; i.e., $\mathbf{P}\bar{\mathbb{C}} = \bar{\mathbb{C}}\mathbf{P}$. Eliminating \mathbf{q}_{n+1} from (5.6) via (5.9), the

remaining system (5.6), after premultiplication by $[\mathbf{Q}^t, \mathbf{Q}^t]$, takes the form

$$\begin{bmatrix} \Xi_1 & \Xi_2 \\ \Xi_3 & \Xi_4 \end{bmatrix} \begin{bmatrix} \xi_n \\ \xi_m \end{bmatrix}_{n+1} = \begin{bmatrix} \xi_n^{\text{trial}} \\ \xi_m^{\text{trial}} \end{bmatrix}_{n+1}, \quad (5.12)$$

where

$$\xi_n := \mathbf{Q}^t \eta_n, \quad \xi_m := \mathbf{Q}^t \eta_m \quad (5.13)$$

and

$$\begin{aligned} \Xi_1(\gamma^1, \gamma^2)_{n+1} &:= \mathbf{1}_3 + (\gamma^1 + \gamma^2)_{n+1} \frac{2}{n_0^2} \left[\frac{4}{3} H' \mathbf{A}_P + h \mathbf{A}_{\bar{C}} \mathbf{A}_P \right], \\ \Xi_2(\gamma^1, \gamma^2)_{n+1} &:= (\gamma^1 - \gamma^2)_{n+1} \frac{1}{\sqrt{3} n_0 m_0} \left[\frac{4}{3} H' \mathbf{A}_P + h \mathbf{A}_{\bar{C}} \mathbf{A}_P \right], \\ \Xi_3(\gamma^1, \gamma^2)_{n+1} &:= (\gamma^1 - \gamma^2)_{n+1} \frac{1}{\sqrt{3} n_0 m_0} \left[\frac{4}{3} H' \mathbf{A}_P + \frac{h^3}{12} \mathbf{A}_{\bar{C}} \mathbf{A}_P \right], \\ \Xi_4(\gamma^1, \gamma^2)_{n+1} &:= \mathbf{1}_3 + (\gamma^1 + \gamma^2)_{n+1} \frac{2}{m_0^2} \left[\frac{4}{3} H' \mathbf{A}_P + \frac{h^3}{12} \mathbf{A}_{\bar{C}} \mathbf{A}_P \right]. \end{aligned} \quad (5.14)$$

Inversion of (5.12) leads to

$$\begin{bmatrix} \xi_n \\ \xi_m \end{bmatrix}_{n+1} = \begin{bmatrix} \bar{\Xi}_1 & \bar{\Xi}_2 \\ \bar{\Xi}_3 & \bar{\Xi}_4 \end{bmatrix} \begin{bmatrix} \xi_n^{\text{trial}} \\ \xi_m^{\text{trial}} \end{bmatrix}_{n+1}, \quad (5.15)$$

where $\bar{\Xi}_k$, $k \in \{1, \dots, 4\}$, are diagonal and are given by

$$\begin{aligned} \bar{\Xi}_3(\gamma^1, \gamma^2)_{n+1} &:= [\Xi_2 - \Xi_1 \Xi_3^{-1} \Xi_4]^{-1}, \\ \bar{\Xi}_4(\gamma^1, \gamma^2)_{n+1} &:= [\Xi_4 - \Xi_3 \Xi_1^{-1} \Xi_2]^{-1}, \\ \bar{\Xi}_1(\gamma^1, \gamma^2)_{n+1} &:= -\Xi_3^{-1} \Xi_4 \bar{\Xi}_3, \\ \bar{\Xi}_2(\gamma^1, \gamma^2)_{n+1} &:= -\Xi_1^{-1} \Xi_2 \bar{\Xi}_4. \end{aligned} \quad (5.16)$$

With these results at hand, $f_{\mu, n+1}$, $\mu \in \{1, 2\}$, may be expressed as

$$f_{\mu, n+1} = \begin{bmatrix} \xi_n \\ \eta_q \\ \xi_m \end{bmatrix}_{n+1}^t \boldsymbol{\Omega}_\mu \begin{bmatrix} \xi_n \\ \eta_q \\ \xi_m \end{bmatrix}_{n+1}, \quad (5.17)$$

where

$$\boldsymbol{\Omega}_\mu := \begin{bmatrix} \frac{1}{n_0^2} \mathbf{A}_P & \mathbf{0} & \frac{\text{sign}(\mu)}{2\sqrt{3}n_0m_0} \mathbf{A}_P \\ \mathbf{0} & \frac{1}{q_0^2} \mathbf{1}_2 & \mathbf{0} \\ \frac{\text{sign}(\mu)}{2\sqrt{3}n_0m_0} \mathbf{A}_P & \mathbf{0} & \frac{1}{m_0^2} \mathbf{A}_P \end{bmatrix}. \quad (5.18)$$

Substituting (5.9) and (5.15) into (5.17) leads to

$$\hat{f}_\mu(\gamma^1, \gamma^2)_{n+1} := \begin{bmatrix} \xi_n^{\text{trial}} \\ \eta_q^{\text{trial}} \\ \xi_m^{\text{trial}} \end{bmatrix}_{n+1}^\text{t} \mathbb{S}^i(\gamma^1, \gamma^2)_{n+1} \boldsymbol{\Omega}_\mu \mathbb{S}(\gamma^1, \gamma^2)_{n+1} \begin{bmatrix} \xi_n^{\text{trial}} \\ \eta_q^{\text{trial}} \\ \xi_m^{\text{trial}} \end{bmatrix}_{n+1}, \quad (5.19)$$

where

$$\mathbb{S}(\gamma^1, \gamma^2)_{n+1} := \begin{bmatrix} \bar{\Xi}_1 & \mathbf{0} & \bar{\Xi}_2 \\ \mathbf{0} & \zeta_{n+1} \mathbf{1}_2 & \mathbf{0} \\ \bar{\Xi}_3 & \mathbf{0} & \bar{\Xi}_4 \end{bmatrix}_{n+1}. \quad (5.20)$$

In (5.19), only $\mathbb{S}(\gamma^1, \gamma^2)_{n+1}$ is dependent on γ_{n+1}^μ , $\mu = 1, 2$. Next, it follows from (5.1)₅, (5.3)₂ and (4.13) that, for plastic loading,

$$\begin{aligned} \hat{p}(\gamma^1, \gamma^2)_{n+1} &:= p_n + \sum_{\mu \in \{1, 2\}} \gamma_{n+1}^\mu 2 \frac{\hat{\kappa}(\gamma^1, \gamma^2)_{n+1}}{\kappa_0} \\ &= p_n + \sum_{\mu \in \{1, 2\}} \gamma_{n+1}^\mu 2 \sqrt{\hat{f}_\mu(\gamma^1, \gamma^2)_{n+1}}, \end{aligned} \quad (5.21)$$

where

$$\hat{\kappa}(\gamma^1, \gamma^2)_{n+1} := \kappa_0 \sqrt{\hat{f}_\mu(\gamma^1, \gamma^2)_{n+1}}. \quad (5.22)$$

The yield functions, $\phi_{\mu, n+1}$, may then be expressed exclusively in $\{\gamma^1, \gamma^2\}_{n+1}$ as

$$\hat{\phi}_\mu(\gamma^1, \gamma^2)_{n+1} = \hat{f}_\mu(\gamma^1, \gamma^2)_{n+1} - \frac{\hat{\kappa}^2(\gamma^1, \gamma^2)_{n+1}}{\kappa_0^2} = 0, \quad \mu = 1, 2. \quad (5.23)$$

Consequently, (5.23) replaces (5.5) as a reduced nonlinear, rank-2 system for γ^μ , $\mu = 1, 2$ subject to the unilateral constraints (5.2). It may be shown that $\hat{\phi}_{\mu, n+1}$, $\mu = 1, 2$ monotonically decrease with γ_{n+1}^μ , $\mu = 1, 2$ and that

$$\lim_{\{\gamma^1, \gamma^2\} \rightarrow 0} \hat{\phi}_{\mu, n+1} = 0, \quad \mu = 1, 2. \quad (5.24)$$

Thus, for monotonically increasing hardening laws, (5.23) has a *unique* solution $\gamma_{n+1}^1 \geq 0$, $\gamma_{n+1}^2 \geq 0$. An iterative solution procedure to solve (5.23) is discussed below.

5.2.2. Iterative solution scheme

The reduced system (5.23) is ideally suited for a local iterative solution scheme using Newton's method. The crucial difference between the solution algorithm for the multi-surface system (5.23) and standard solution algorithms for analogous single surface systems concerns the determination of the active surfaces during the return mapping. For convenience, the iterative solution algorithm for the solution of (5.23) subject to the unilateral constraints (5.2) is summarized in Boxes 1–4, in which,

$$\partial_{\gamma^\beta} \hat{f}_{\mu, n+1} = 2 \begin{bmatrix} \xi_n^{\text{trial}} \\ \eta_q^{\text{trial}} \\ \xi_m^{\text{trial}} \end{bmatrix}_{n+1}^\text{t} (\mathbb{S}_{n+1})^i \boldsymbol{\Omega}_\mu (\partial_{\gamma^\beta} \mathbb{S}_{n+1}) \begin{bmatrix} \xi_n^{\text{trial}} \\ \eta_q^{\text{trial}} \\ \xi_m^{\text{trial}} \end{bmatrix}_{n+1}, \quad (5.25)$$

Box 4. (Continued) Newton iteration for γ^1, γ^2

7. Update γ^μ

$$\bar{\gamma}_{n+1}^{\mu(k+1)} := \gamma_{n+1}^{\mu(k)} + \Delta\gamma_{n+1}^{\mu(k)} [\text{trial } \gamma^\mu]$$

IF: $\bar{\gamma}_{n+1}^{\mu(k+1)} < 0, \mu \in \mathbb{J}_{\text{act}}^{(k)}$, THEN:

$$\text{Reset } \mathbb{J}_{\text{act}}^{(k+1)} = \{\mu \in \mathbb{J}_{\text{act}}^{(k)} \mid \bar{\gamma}_{n+1}^{\mu(k+1)} > 0\}$$

Set $k = k + 1$ and GO TO 3

ELSE:

$$\gamma_{n+1}^{\mu,(k+1)} = \bar{\gamma}_{n+1}^{\mu,(k+1)}$$

Set $k = k + 1$ and GO TO 4

ENDIF.

where

$$\partial_{\gamma^\beta} \mathbb{S} = \begin{bmatrix} \frac{2}{n_0^2} \left[\frac{4}{3} H' \Lambda_P + h \Lambda_{\bar{C}} \Lambda_P \right] & \mathbf{0} & \frac{\text{sign}(\beta)}{\sqrt{3} n_0 m_0} \left[\frac{4}{3} H' \Lambda_P + h \Lambda_{\bar{C}} \Lambda_P \right] \\ \mathbf{0} & \partial_{\gamma^\beta} \zeta_{n+1} \mathbf{1}_2 & \mathbf{0} \\ \frac{\text{sign}(\beta)}{\sqrt{3} n_0 m_0} \left[\frac{4}{3} H' \Lambda_P + \frac{h^3}{12} \Lambda_{\bar{C}} \Lambda_P \right] & \mathbf{0} & \frac{2}{m_0^2} \left[\frac{4}{3} H' \Lambda_P + \frac{h^3}{12} \Lambda_{\bar{C}} \Lambda_P \right] \end{bmatrix},$$

$$\partial_{\gamma^\beta} \zeta_{n+1} = \frac{-Gh\kappa \frac{2}{q_0^2}}{1 + Gh\kappa \frac{2}{q_0^2} (\gamma_{n+1}^1 + \gamma_{n+1}^2)}. \quad (5.26)$$

Note that special precaution is required when $\langle \mathbf{n}, \mathbf{m} \rangle_P \equiv 0$; $\langle \mathbf{n}, \mathbf{m} \rangle_P := \mathbf{n}^T \mathbf{P} \mathbf{m}$, since the matrix \mathbf{g} in Box 3 becomes singular in this case. Once $\gamma^\mu, \mu = 1, 2$ are determined from the solution of (5.23), the remaining state variables are obtained from (5.21), (5.15), (5.14)₁, (5.1) and (5.2) as follows:

$$\begin{Bmatrix} \boldsymbol{\eta}_n \\ \boldsymbol{\eta}_q \\ \boldsymbol{\eta}_m \end{Bmatrix}_{n+1} = \begin{bmatrix} Q \bar{\Xi}_1 & \mathbf{0} & Q \bar{\Xi}_2 \\ \mathbf{0} & \zeta_{n+1} \mathbf{1}_2 & \mathbf{0} \\ Q \bar{\Xi}_3 & \mathbf{0} & Q \bar{\Xi}_4 \end{bmatrix}_{n+1} \begin{Bmatrix} \boldsymbol{\xi}_n^{\text{trial}} \\ \boldsymbol{\eta}_q^{\text{trial}} \\ \boldsymbol{\xi}_m^{\text{trial}} \end{Bmatrix}_{n+1},$$

$$\boldsymbol{\varepsilon}_{n+1}^P = \boldsymbol{\varepsilon}_n^P + \sum_{\mu \in \{1,2\}} \gamma_{n+1}^\mu 2 \mathbf{A}_\mu \boldsymbol{\eta}_{n+1}, \quad (5.27)$$

$$\mathbf{p}_{n+1} = \begin{Bmatrix} p \\ \bar{p} \end{Bmatrix}_{n+1} = \begin{Bmatrix} p_n + \sum_{\mu \in \{1,2\}} \gamma_{n+1}^\mu \frac{2 \hat{\kappa}(\gamma^1, \gamma^2)_{n+1}}{\kappa_0} \\ -\frac{2}{3} H' \boldsymbol{\varepsilon}_{n+1}^P \end{Bmatrix}.$$

The stress resultants are then obtained from $\boldsymbol{\sigma}_{n+1} = \boldsymbol{\eta}_{n+1} - \bar{\mathbf{p}}_{n+1}$.

5.3. Algorithmic elastoplastic tangent moduli

The linearization of the *weak form* (2.37) is completed by specifying the form of $d\sigma_{n+1}/d\epsilon_{n+1}$; i.e. the *consistent* elastoplastic tangent moduli. An important advantage of the algorithm summarized in Boxes 1–4 is that it can be exactly *linearized in closed form* to obtain these consistent tangent moduli. Use of convected coordinates allows the tangent moduli to take a remarkably simple form. In fact, in matrix notation, the form is identical to that in the kinematically linear theory. Restricting our attention to isotropic hardening, the linearization of the return mapping algorithm leads, in matrix notation, to the following *algorithmic elastoplastic tangent moduli*:

$$\frac{d\sigma}{d\epsilon} \Big|_{n+1} = \mathbf{E}_{\sigma_{n+1}} - \sum_{\beta \in \mathbb{J}_{act}} \sum_{\alpha \in \mathbb{J}_{act}} g_{n+1}^{\beta\alpha} \mathbf{N}_{\beta,n+1} \mathbf{N}_{\alpha,n+1}^t, \quad (5.28)$$

where

$$\begin{aligned} E_{p_{n+1}} &:= \left[D^{-1} + \sum_{\alpha=1}^m \gamma_{n+1}^\alpha \partial_{pp}^2 \phi_\alpha \right]^{-1}, \\ \mathbf{E}_{\sigma_{n+1}} &:= \left[\mathbb{C}_{n+1}^{-1} + \sum_{\alpha=1}^m \gamma_{n+1}^\alpha \partial_{\sigma\sigma}^2 \phi_{\alpha,n+1} \right]^{-1}, \\ g_{n+1}^{\beta\alpha} &:= -[(\partial_\sigma \phi_{\beta,n+1})^t \mathbf{E}_{\sigma_{n+1}} (\partial_\sigma \phi_{\alpha,n+1}) + \partial_p \phi_{\beta,n+1} E_{p_{n+1}} \partial_p \phi_{\alpha,n+1}]^{-1}, \\ N_{\alpha,n+1} &:= -\mathbf{E}_{\sigma_{n+1}} \partial_\sigma \phi_{\alpha,n+1}. \end{aligned} \quad (5.29)$$

We remark that the structure of (5.28) is entirely analogous to the expression for the continuum elastoplastic tangent moduli. To obtain the *continuum* tangent moduli all that is needed is to replace the *algorithmic* moduli $\mathbf{E}_{\sigma_{n+1}}$ in the expression for the *algorithmic* elastoplastic moduli by the elastic moduli \mathbb{C}_{n+1} . A derivation of (5.28) as well as a similar result for the case of combined isotropic/kinematic hardening are provided in Appendix A. With $d\sigma_{n+1}/d\epsilon_{n+1}$ specified here, the linearization of the *discrete* weak form (2.37) is fully defined. This consistent linearization of the weak form leads not only to quadratic rates of asymptotic convergence in a global Newton iteration scheme, but also to robust continuation methods for post-buckling analysis such as those discussed in Part III.

6. Numerical examples

Four numerical examples are considered to illustrate both the physical behavior of the shell under the proposed generalization to the Ilyushin–Shapiro yield criterion as well as the performance of the corresponding return mapping algorithm. The objective of these simulations is to demonstrate the reliable performance of the new plasticity model and its implementation in practical calculations. All calculations are performed on a Convex C1 computer by implementing the algorithm in Boxes 1–4 in an enhanced version of the nonlinear finite element computer program FEAP, developed by R.L. Taylor, and described in Chapter 24 of [22]. A global Newton solution procedure enhanced with a line search algorithm is used throughout. The finite element spatial discretization consists of 4-node isoparametric quadrilateral elements with bilinear displacement interpolation and 2×2 Gaussian quadrature. Attention is directed toward the excellent convergence characteristics of the

global Newton procedure due to use of the consistent tangent operator developed in Section 5.3.

6.1. Built-in, perfectly plastic beam

A perfectly plastic beam built in on each end with a concentrated load at the $\frac{3}{4}$ point along its span is considered first. The geometry, material properties and finite element mesh, consisting of 60 elements with added refinement neighboring the locations of the onset of plastic hinges, are shown in Fig. 4. The objective here is to compare the global response predicted by the shell model with the Bernoulli-Euler (bending dominated) elementary analytical solution (see e.g., [23]) in predicting the onset of plastic hinges. Consequently, only the shell model with linear kinematics is considered (see Part II). Furthermore, the rigidities associated with membrane (Eh), bending ($Eh^3/12$) and transverse shear ($Gh\kappa$) response are taken as independent parameters in order to simulate the elementary bending dominated solution. Similarly, the yield parameters n_0 , m_0 and q_0 are also treated independently.

The transverse load P applied to the beam is plotted against the transverse displacement under the load in Fig. 5. The break points in the plot associated with the elementary solution correspond to the formation of plastic hinges, first at the boundary closest to the load application, and next at the point of the load application. A third hinge forming at the boundary furthest from the load corresponds to the collapse load of the beam. The effect of the shell model, as is evident in Fig. 5, is to smooth or blunt these break points upon formation of plastic hinges. The mechanism for this smoothing process is depicted in Fig. 6. Elastic loading occurs along the m_{11} axis until the first yielding occurs at $m_{11} = m_0$. Next, in contrast to the elementary solution which relies on a one-dimensional yield criterion and stress state, further increase of the load P allows additional increases in m_{11} (pseudo-hardening) as well as nonzero values of m_{22} due to the orthogonal projection of the trial state onto the yield surface. Consequently, m_{11} and m_{22} are allowed to increase progressively through points B and D. Hence, locally in the beam, the multi-dimensional nature of the shell yield criterion acts as a pseudo-hardening mechanism from point A to D in Fig. 6. An analogous process occurs at subsequent hinge points. Furthermore, the shell yield criterion serves to distribute the plastic zone neighboring each hinge through a finite longitudinal region, in contrast to the longitudinally point-wise hinges predicted in the elementary solution. In spite of these differences, there is good overall qualitative agreement between the two solutions.

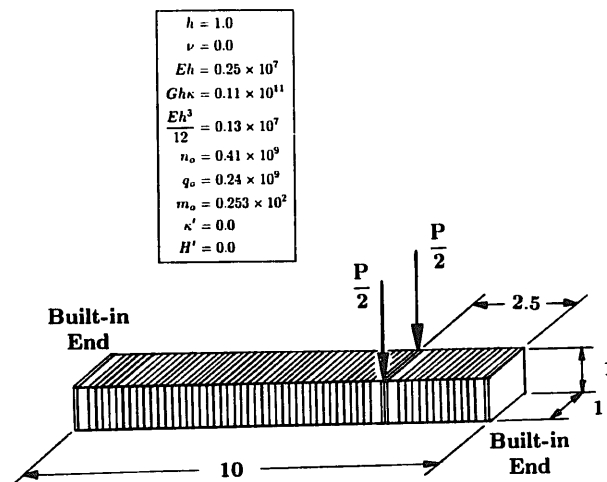


Fig. 4. Geometry, finite element mesh and material properties for a built-in, perfectly plastic beam.

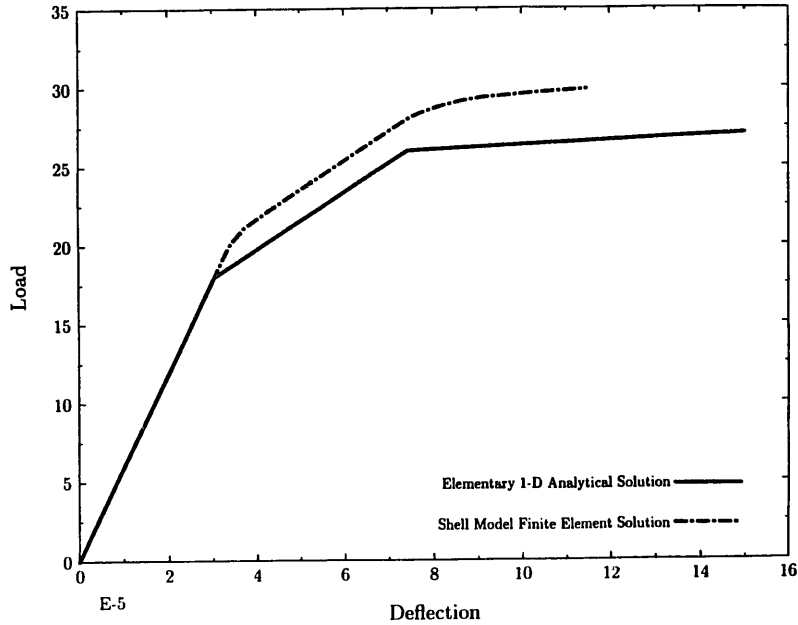
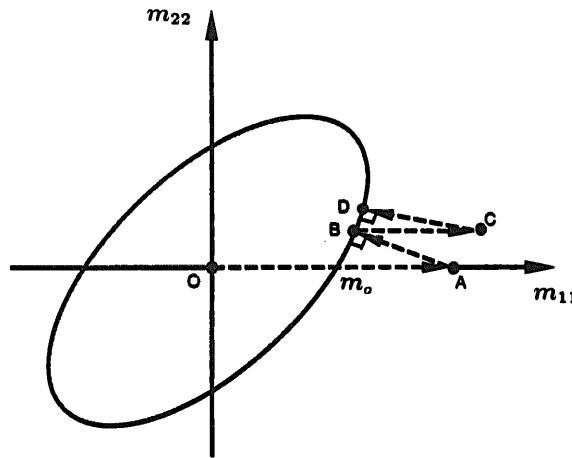


Fig. 5. Load-displacement curves for a built-in beam: elementary moment dominated analytical solution, and bending dominated shell model solution.



6.2. Point-loaded, simply supported, perfectly plastic plate

A perfectly plastic, simply supported plate with a point load at its center is considered next. Due to symmetry, only $\frac{1}{4}$ of the plate will be considered. The $\frac{1}{4}$ domain geometry, material properties and finite element mesh, consisting of 1200 elements with added refinement neighboring the locations of the onset of diagonal plastic hinges, are shown in Fig. 7. The objective here is to compare the shell response to the predictions of the elementary bending dominated limit load analysis (see e.g. [23]) within the context of the Kirchhoff–Love kinematic hypothesis. Consequently, as with the beam in Section 6.1, only linear kinematics is considered and the rigidities and yield parameters associated with membrane, bending and transverse shear response are treated as independent parameters. The transverse load P applied to the $\frac{1}{4}$ plate is plotted against the transverse displacement under the load in Fig. 8.

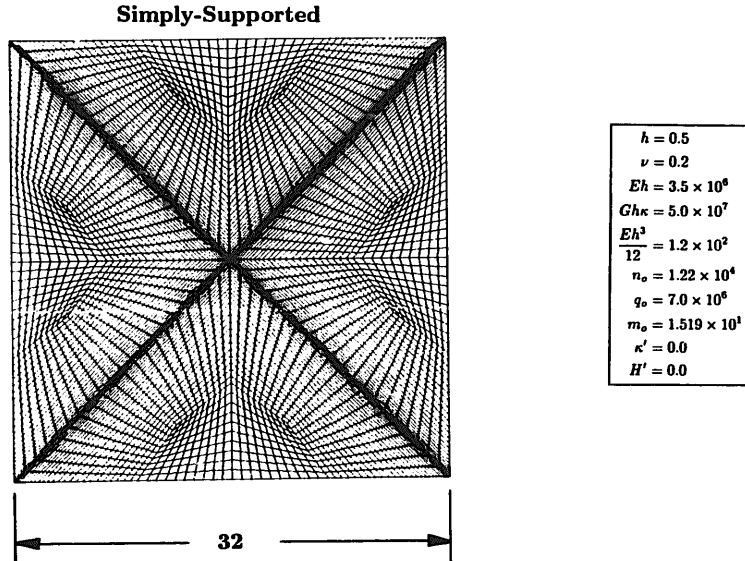


Fig. 7. Geometry, finite element mesh and material properties for a point-loaded, simply supported perfectly plastic plate.

Note that the load values shown in this figure are $\frac{1}{4}$ of the load applied to the corresponding full plate due to the enforcement of the symmetry conditions. As shown in the figure, the elastic solution matches the elementary Kirchhoff–Love plate theory solution identically (see [24, p. 143]). The plastic solution also shows good qualitative agreement with the upper bound on the limit load obtained using classical elementary methods (see e.g. [23]).⁶ Again, as in the beam example above, the physical influence of the shell yield criterion is to provide a smooth transition between the elasticity dominated and plasticity dominated solutions.

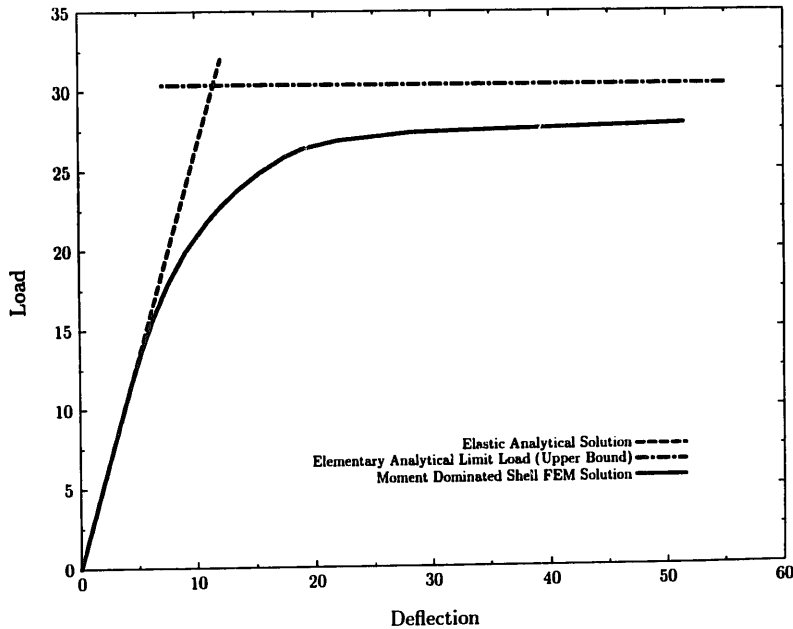


Fig. 8. Load–displacement curves for a simply supported plate: elementary Kirchhoff–Love elastic solution appended to elementary upperbound plastic collapse solution, and bending dominated shell model solution.

⁶ It is useful to note that better bounds (upper and lower) are available for the *uniformly* loaded plate problem in [25]. This was kindly brought to our attention by one of the reviewers of this manuscript.

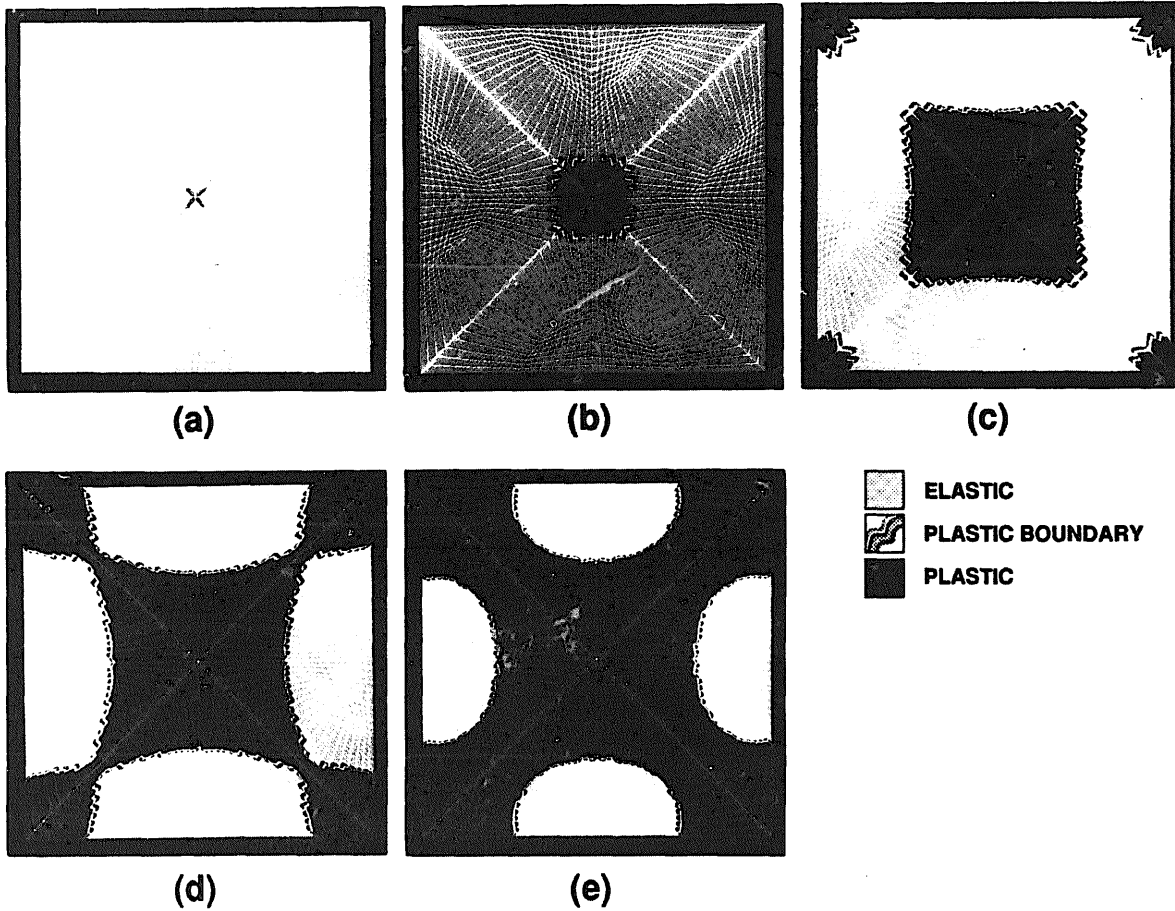


Fig. 9. Evolution of plastic zone in a simply-supported plate: (a) $P = 11.0$; (b) $P = 18.5$; (c) $P = 25.6$; (d) $P = 26.3$; (e) $P = 27.0$.

The evolution of the plastic zone in the plate is depicted in Fig. 9(a–e) for increasing loads. Note that, although the elementary limit load analysis assumes that the plastic hinges occur along infinitely thin lines, the shell model predicts finite width plastic zones neighboring each hinge, a direct analog to the finite zones in the beam. These plastic zones have considerable width in comparison to the plate thickness, even for a highly refined in-plane mesh, as is shown in Fig. 9(d–e). Nevertheless, there again is good qualitative agreement between the two solutions.

6.3. Pinched cylinder with isotropic hardening

As a third example, a short cylinder bounded by two rigid diaphragms at its ends, loaded with two radial pinching displacements at the middle section, and characterized by an isotropic hardening plastic response is considered. Due to symmetry, only one octant of the cylinder is modeled. The geometry, material properties and finite element mesh of the octant, consisting of 1024 equally spaced elements, are shown in Fig. 10. Full finite deformation kinematics are considered here.

The pinching loading P is plotted against the radial displacement under the load in Fig. 11. The step-like regions are due to snap-through-like mechanisms which arise as a result of the relatively coarse mesh in comparison to the width of the indentation ridge forming about the

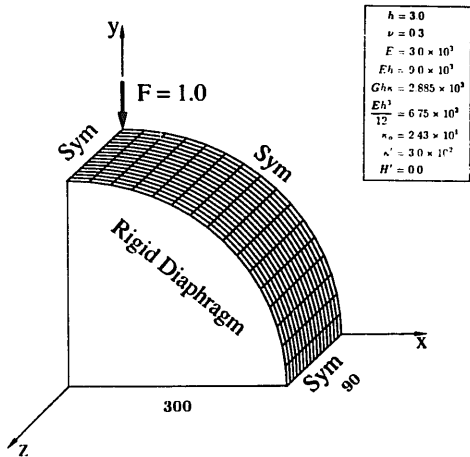


Fig. 10 Geometry, finite element mesh and material properties for pinched cylinder.

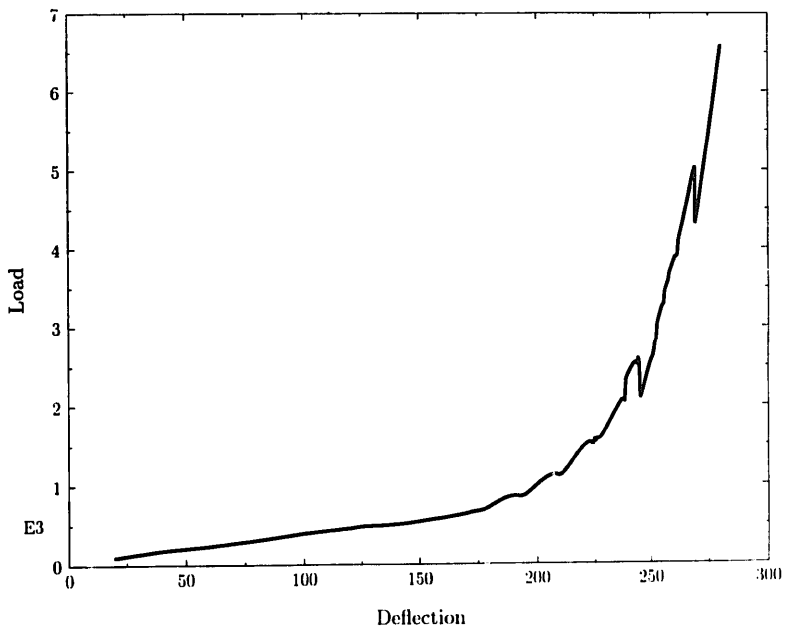


Fig. 11. Load-displacement curve for a pinched cylinder.

point load upon loading (see Fig. 12(c–e)). That is, such regions are due to the nature in which the ridge, which has a width equal to or below the element width, passes through the elements as the ridge moves outward. Note that the pinching displacement in the final configuration is nearly the cylinder radius. Progressive states of the deformed configuration as well as the evolution of the plastic zone in the cylinder are shown in Fig. 12.

6.4. Pinched hemisphere with isotropic hardening

A hemisphere bounded by a free edge, loaded by two inward and two outward forces 90° apart, and characterized by an isotropic hardening plastic response is considered last. Due to symmetry, only one quadrant of the hemisphere is modeled. The geometry, material properties and finite element mesh of the quadrant, consisting of 768 elements, are shown in

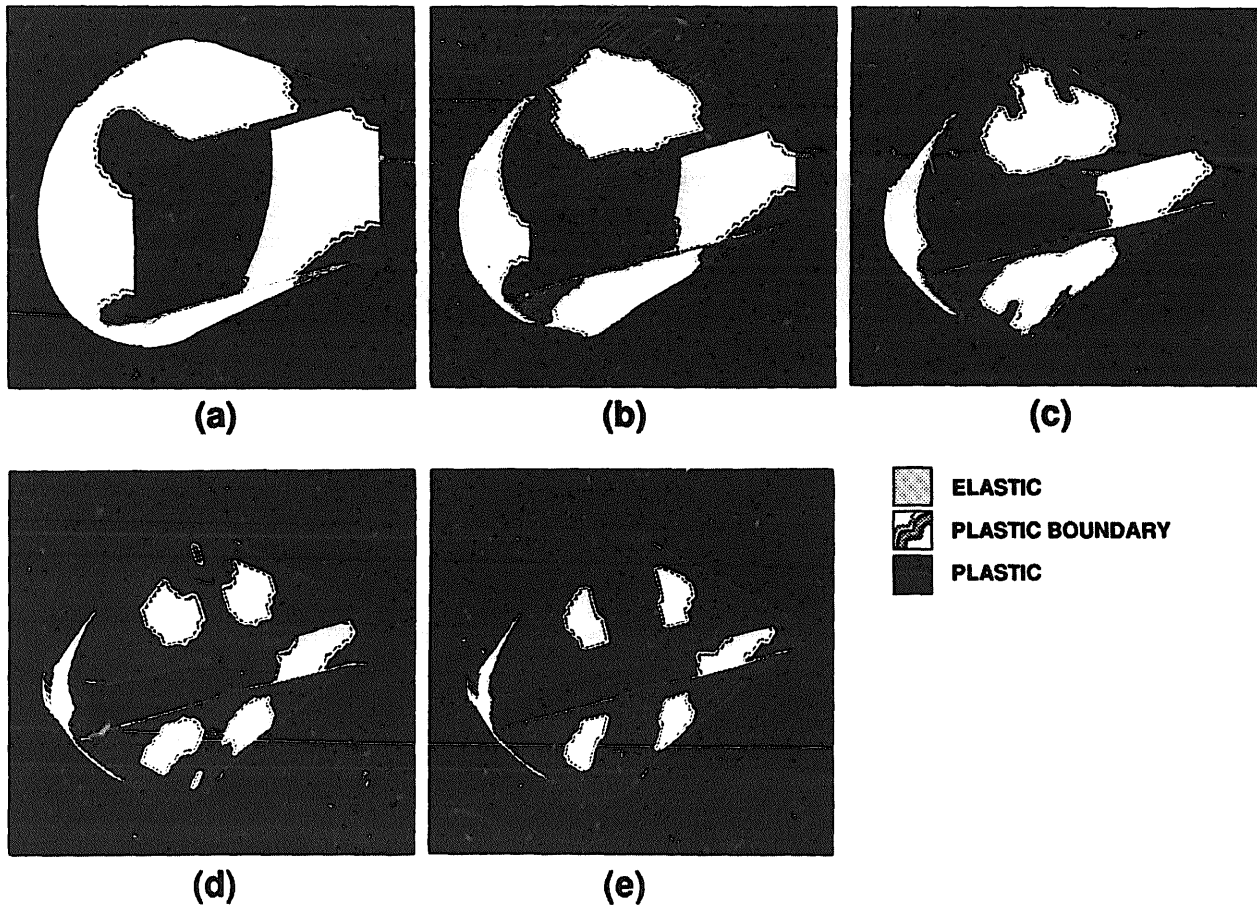


Fig. 12. Evolution of plastic zone in a pinched cylinder: (a) $\bar{u} = 150$; (b) $\bar{u} = 207$; (c) $\bar{u} = 247$; (d) $\bar{u} = 268$; (e) $\bar{u} = 280$.

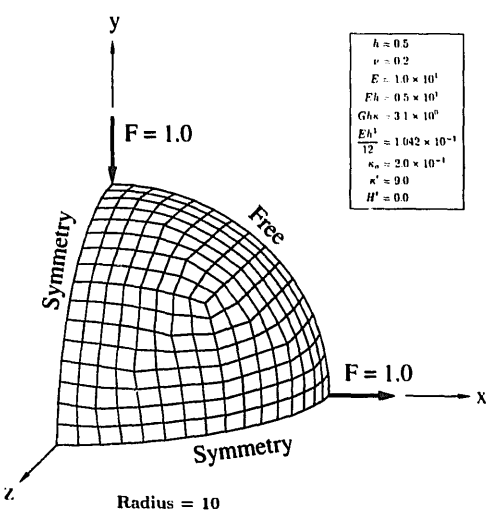


Fig. 13. Geometry, finite element mesh and material properties for a pinched sphere.

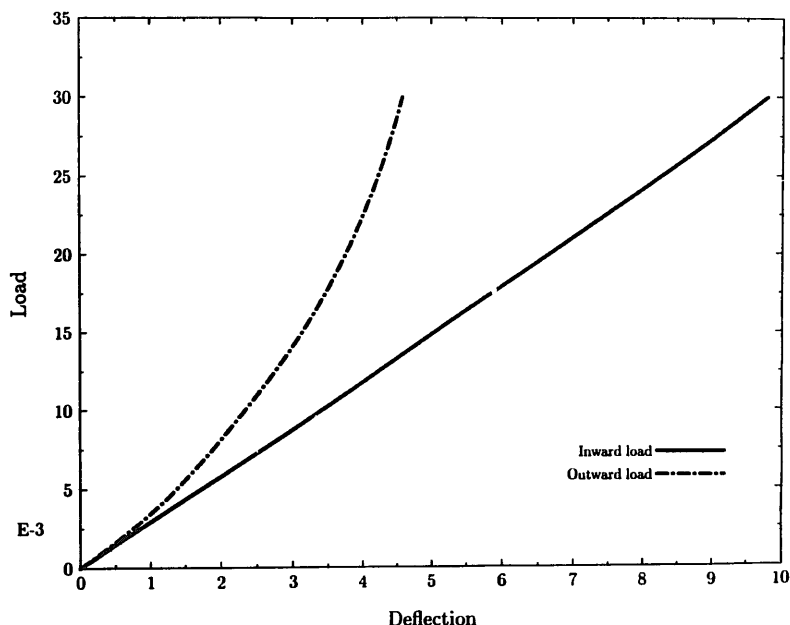


Fig. 14. Load-displacement curves for pinched sphere: inward load and outward load.

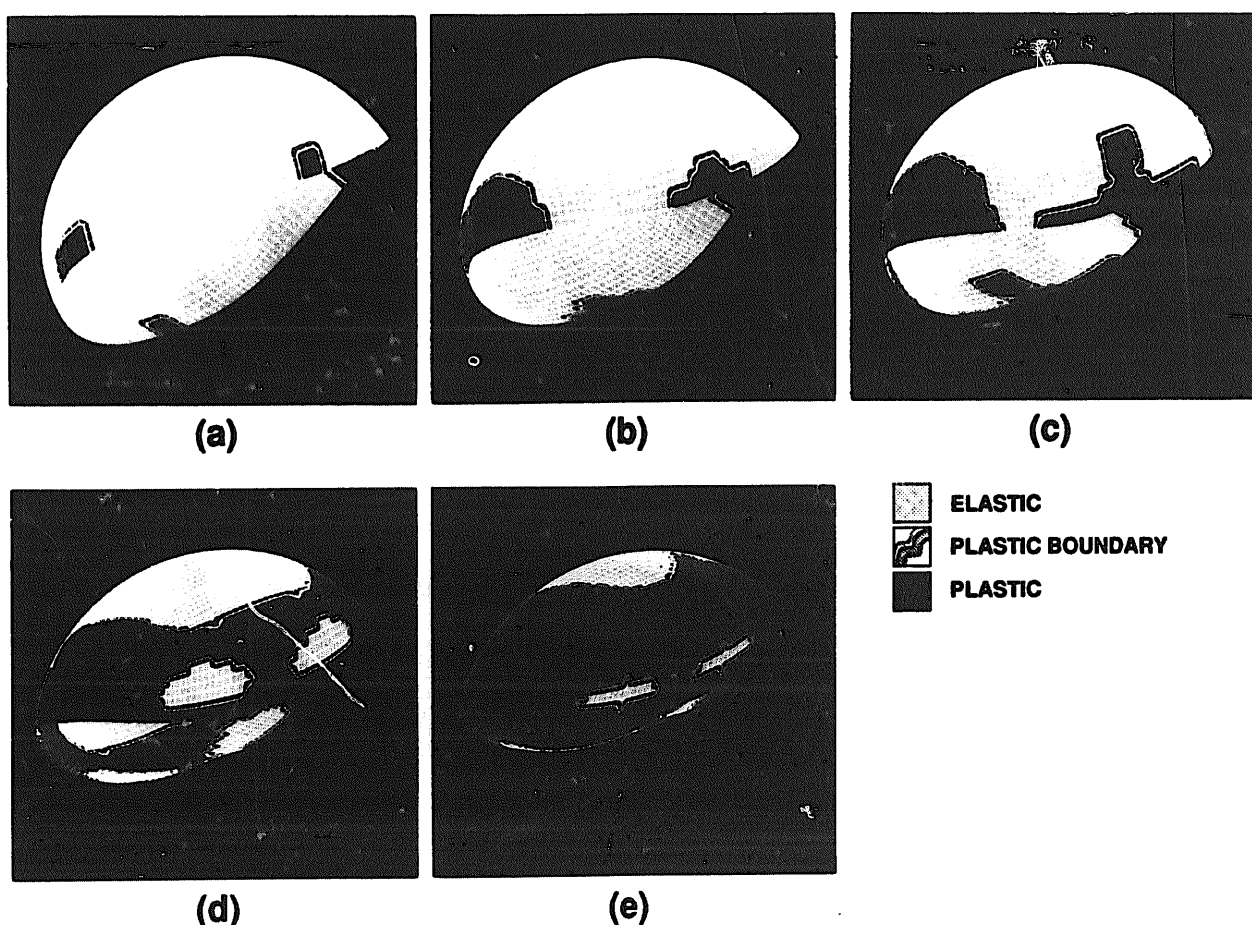


Fig. 15. Evolution of plastic zone for a pinched sphere: (a) $P = 0.010$; (b) $P = 0.016$; (c) $P = 0.019$; (d) $P = 0.023$; (e) $P = 0.029$.

Fig. 13. As with the cylinder in Section 6.3, full finite deformation kinematics are represented here.

The applied loads P are plotted against the radial displacement under each respective load in Fig. 14. Note that the inward displacement in the final configuration is nearly equal to the hemisphere radius. Progressive states of the deformed configuration as well as the evolution of the plastic zone in the hemisphere are shown in Fig. 15.

6.5. Convergence rates for global Newton iterations

Use of the exact, closed-form consistent tangent operator developed in Section 5.3 leads to quadratic rates of asymptotic convergence in a global Newton iterative procedure. These excellent convergence properties are present even for reasonably large problems such as those considered in Sections 6.2, 6.3 and 6.4. As an illustration, values of the Euclidean norm of the global residual are reported in Tables 2 and 3 within typical plastic load steps for the examples in Sections 6.3 and 6.4. These results clearly exhibit the quadratic rates of asymptotic convergence.

Table 2
Pinched cylinder: residual norms for global Newton iteration

Iteration	Load step			
	$P = 200^a$	$P = 690$	$P = 2491$	$P = 8753$
1	0.254E + 06	0.516E + 04	0.375E + 04	0.350E + 04
2	0.105E + 05	0.919E + 02	0.211E + 03	0.964E + 02
3	0.127E + 04	0.202E + 00	0.250E + 01	0.792E + 00
4	0.445E + 03	0.526E - 04	0.263E + 00	0.172E - 04
5	0.962E + 02	0.191E - 07	0.121E - 04	0.182E - 07
6	0.143E + 02	-	0.190E - 07	-
7	0.169E + 00	-	-	-
8	0.607E - 04	-	-	-
9	0.214E - 07	-	-	-

^a Elastic step (larger time step).

Table 3
Pinched hemisphere: residual norms for global Newton iteration

Iteration	Load step			
	$P = 0.006^a$	$P = 0.015$	$P = 0.021$	$P = 0.029$
1	0.212E - 02	0.212E - 02	0.212E - 02	0.212E - 02
2	0.419E - 01	0.314E - 01	0.324E - 01	0.314E - 01
3	0.365E - 03	0.179E - 02	0.437E - 02	0.109E - 01
4	0.115E - 04	0.248E - 04	0.354E - 03	0.102E - 02
5	0.213E - 08	0.595E - 09	0.289E - 04	0.442E - 04
6	-	-	0.124E - 08	0.214E - 05
7	-	-	-	0.240E - 10

^a Elastic step (larger time step).

7. Concluding remarks

Within, the context of the geometrically exact shell model discussed in Part III of this work, the formulation and numerical implementation of a general constitutive theory for elastoplasticity formulated entirely in terms of stress resultants and stress couples has been presented. As an application, an extension of the classical Ilyushin–Shapiro yield criterion to include both kinematic and isotropic hardening has been considered. The return mapping algorithm circumvents the use of objective integrators to define the trial stress, is unconditionally stable, involves only the solution of two nonlinear scalar equations at the stress-point level, and is amenable to exact linearization.

Future work will extend the present formulation in two directions. From a physical modeling perspective, the theory and finite element method is generalized to include transient temporal response. From a numerical analysis perspective, an *assumed stress method* is developed for the elastoplastic problem which possesses identical accuracy for coarse meshes in elastic problems as the assumed stress method considered in Part III for the membrane and bending fields. This new assumed stress method has the advantage of requiring *no modification* of the return mapping algorithm (at the stress-point level) discussed within the context of a displacement formulation in Section 5.

Acknowledgment

We are indebted to M.S. Rifai for his involvement in the numerical implementation of the formulation described in this paper. Support for this research was provided by AFOSR Grants AFOSR-86-0292, AFOSR-28169-A and LLNL Grant LLNL-2254903 with Stanford University. J.G. Kennedy was supported by a Fellowship from the Shell Development Company. This support is gratefully acknowledged.

Appendix A. Linearization: algorithmic tangent moduli

The exact linearization of the return mapping algorithm summarized in Boxes 1–4 is sketched below. For simplicity, the development will consider only isotropic hardening, although the end result for combined isotropic/kinematic hardening will also be reported.

Differentiation of the elastic stress-strain relations (4.12)₁ and the discrete flow rule (5.1)₂ yields (noting that $\partial_{\sigma p} \phi_\alpha(\sigma, p) = 0$ for strictly isotropic hardening)

$$\begin{aligned} d\sigma_{n+1} &= C_{n+1}(d\epsilon_{n+1} - d\epsilon_{n+1}^p), \\ d\epsilon_{n+1}^p &= \sum_{\alpha=1}^m [\gamma_{n+1}^\alpha \partial_{\sigma\sigma}^2 \phi_\alpha(\sigma, p)_{n+1} d\sigma_{n+1} + d\gamma_{n+1}^\alpha \partial_\sigma \phi_\alpha(\sigma, p)_{n+1}]. \end{aligned} \quad (\text{A.1})$$

By combining these two equations one obtains the relation

$$d\sigma_{n+1} = E_{\sigma_{n+1}} \left[d\epsilon_{n+1} - \sum_{\alpha=1}^m d\gamma_{n+1}^\alpha \partial_\sigma \phi_\alpha(\sigma, p)_{n+1} \right], \quad (\text{A.2})$$

where $E_{\sigma_{n+1}}$ are *algorithmic* moduli now given by the expression

$$E_{\sigma_{n+1}} := \left[C_{n+1}^{-1} + \sum_{\alpha=1}^m \gamma_{n+1}^\alpha \partial_{\sigma\sigma}^2 \phi_{\alpha_{n+1}} \right]^{-1}. \quad (\text{A.3})$$

Similarly, differentiation of the discrete hardening law (5.1)₃ yields

$$\begin{aligned} dp_{n+1} &= -E_{p_{n+1}} \sum_{\alpha=1}^m d\gamma_{n+1}^\alpha \partial_p \phi_{\alpha,n+1}, \\ E_{p_{n+1}} &:= \left[D^{-1} + \sum_{\alpha=1}^m \gamma_{n+1}^\alpha \partial_{pp}^2 \phi_\alpha \right]^{-1}. \end{aligned} \quad (\text{A.4})$$

Next, the coefficients $d\gamma_{n+1}^\alpha$ are determined from the algorithmic version of the consistency condition obtained by differentiation $\phi_\alpha(\sigma, p)_{n+1} = 0$; i.e.,

$$(\partial_\sigma \phi_\alpha)^t d\sigma_{n+1} + \partial_p \phi_\alpha dp_{n+1} = 0, \quad \alpha \in \mathbb{J}_{\text{act}}. \quad (\text{A.5})$$

Substitution of (A.2) and (A.4) into (A.5) then yields

$$d\gamma_{n+1}^\beta = \sum_{\alpha \in \mathbb{J}_{\text{act}}} [g_{n+1}^{\beta\alpha}] [(\partial_\sigma \phi_{\alpha,n+1})^t \mathbf{E}_{\sigma_{n+1}} d\epsilon_{n+1}], \quad (\text{A.6})$$

where $g_{n+1}^{\beta\alpha} := [g_{\beta\alpha,n+1}]^{-1}$, and $g_{\beta\alpha,n+1}$ is defined by

$$g_{n+1}^{\beta\alpha} := [(\partial_\sigma \phi_{\beta,n+1})^t \mathbf{E}_{\sigma_{n+1}} \partial_\sigma \phi_{\alpha,n+1} + \partial_p \phi_{\beta,n+1} E_{p_{n+1}} \partial_p \phi_{\alpha,n+1}]^{-1}. \quad (\text{A.7})$$

Finally, substitution of (A.6) into (A.2) gives the desired expression for the algorithmic elastoplastic tangent moduli

$$\begin{aligned} \frac{d\sigma}{d\epsilon} \Big|_{n+1} &= \mathbf{E}_{\sigma_{n+1}} - \sum_{\beta \in \mathbb{J}_{\text{act}}} \sum_{\alpha \in \mathbb{J}_{\text{act}}} g_{n+1}^{\beta\alpha} N_{\beta,n+1}^t N_{\alpha,n+1}, \\ N_{\alpha,n+1} &:= \mathbf{E}_{\sigma_{n+1}} \partial_\sigma \phi_{\alpha,n+1}. \end{aligned} \quad (\text{A.8})$$

A similar calculation for the case of combined isotropic/kinematic hardening leads to the following expression for the algorithmic elastoplastic tangent moduli:

$$\begin{aligned} \frac{d\sigma}{d\epsilon} \Big|_{n+1} &= \mathbf{E}_{\sigma_{n+1}} - \sum_{\beta \in \mathbb{J}_{\text{act}}} \sum_{\alpha \in \mathbb{J}_{\text{act}}} g_{n+1}^{\beta\alpha} N_{\beta,n+1}^t N_{\alpha,n+1}, \\ g_{n+1}^{\beta\alpha} &:= \left[[(\partial_\sigma \phi_\beta)^t, (\partial_\sigma \phi_\beta)^t] \mathbf{E}_{n+1} \left[\begin{array}{c} \partial_\sigma \phi_\alpha \\ \partial_p \phi_\alpha \end{array} \right] + \partial_p \phi_\beta E_{p_{n+1}} \partial_p \phi_\alpha \right]_{n+1}^{-1}, \\ N_{\alpha,n+1} &:= [\bar{\mathbf{E}}_{\sigma_{n+1}} + \bar{\mathbf{E}}_{\tilde{p}_{n+1}}] \partial_\sigma \phi_{\alpha,n+1}. \end{aligned} \quad (\text{A.9})$$

In (A.9), $E_{p_{n+1}}$ is defined in (A.4), \mathbf{E}_{n+1} and $\mathbf{E}_{\sigma_{n+1}}$ are given by

$$\begin{aligned} \mathbf{E}_{n+1} &:= \begin{bmatrix} \mathbb{C}^{-1} + \sum_{\alpha=1}^m \gamma_{n+1}^\alpha \partial_{\sigma\sigma}^2 \phi_{\alpha,n+1} & \sum_{\alpha=1}^m \gamma_{n+1}^\alpha \partial_{\sigma\sigma}^2 \phi_{\alpha,n+1} \\ \sum_{\alpha=1}^m \gamma_{n+1}^\alpha \partial_{\sigma\sigma}^2 \phi_{\alpha,n+1} & \bar{\mathbf{D}}^{-1} + \sum_{\alpha=1}^m \gamma_{n+1}^\alpha \partial_{\sigma\sigma}^2 \phi_{\alpha,n+1} \end{bmatrix}^{-1}, \\ &=: \begin{bmatrix} \mathbf{E}_{\sigma_{n+1}} & \mathbf{E}_{\sigma p_{n+1}} \\ \mathbf{E}_{\sigma \tilde{p}_{n+1}} & \mathbf{E}_{\tilde{p}_{n+1}} \end{bmatrix}^{-1}, \end{aligned} \quad (\text{A.10})$$

and $\bar{\mathbf{E}}_{\sigma_{n+1}}$ and $\bar{\mathbf{E}}_{\sigma \tilde{p}_{n+1}}$ are defined by

$$\mathbf{E}_{n+1}^{-1} =: \begin{bmatrix} \bar{\mathbf{E}}_{\sigma_{n+1}} & \bar{\mathbf{E}}_{\sigma \bar{p}_{n+1}} \\ \bar{\mathbf{E}}_{\sigma \bar{p}_{n+1}} & \bar{\mathbf{E}}_{\bar{p}_{n+1}} \end{bmatrix}. \quad (\text{A.11})$$

In (A.11), \mathbf{E}_{n+1} may be inverted in closed form, analogously to the inversion in (5.15) and (5.16).

Appendix B. Summary of thermodynamic results in elastoplasticity

Here we provide a brief thermodynamic motivation for results cited in Section 4 regarding the elastoplastic constitutive equations. Here, plastic processes are assumed to be fully characterized in terms of the history of three state variables: the *strain measure* components $\boldsymbol{\varepsilon} \in \mathbb{R}^8$, the *plastic strain measure* components $\boldsymbol{\varepsilon}^p \in \mathbb{R}^8$, and a suitable set of *internal variables* $\boldsymbol{\alpha} \in \mathbb{R}^p$ often referred to as *hardening variables*. Accordingly, plastic flow at each point $\mathbf{x} \in \mathcal{B}$ up to the current time $t \in \mathbb{R}_+$ is characterized in terms of the histories $\tau \in (-\infty, t] \mapsto \{\boldsymbol{\varepsilon}(\mathbf{x}, \tau), \boldsymbol{\varepsilon}^p(\mathbf{x}, \tau), \boldsymbol{\alpha}(\mathbf{x}, \tau)\}$. The stress measure components $\boldsymbol{\sigma} \in \mathbb{R}^8$ are then *dependent functions* of the variables $\{\boldsymbol{\varepsilon}, \boldsymbol{\varepsilon}^p\}$ through elastic stress-strain relations, as discussed below.

As discussed in Section 3, the strain measure components $\boldsymbol{\varepsilon} \in \mathbb{R}^8$ are assumed to be *additively decomposed* into an elastic and a plastic part, denoted by $\boldsymbol{\varepsilon}^e \in \mathbb{R}^8$ and $\boldsymbol{\varepsilon}^p \in \mathbb{R}^8$, respectively; i.e.,

$$\boldsymbol{\varepsilon} = \boldsymbol{\varepsilon}^e + \boldsymbol{\varepsilon}^p. \quad (\text{B.1})$$

The *Helmholtz free energy* $\psi : \mathbb{R}^8 \times \mathbb{R}^8 \times \mathbb{R}^p \rightarrow \mathbb{R}$ is assumed to take the form

$$\psi(\boldsymbol{\varepsilon}, \boldsymbol{\varepsilon}^p, \boldsymbol{\alpha}) := W(\boldsymbol{\varepsilon} - \boldsymbol{\varepsilon}^p) + \mathcal{H}(\boldsymbol{\alpha}), \quad (\text{B.2})$$

where $W : \mathbb{R}^8 \rightarrow \mathbb{R}$ is the *elastic stored energy function*, and $\mathcal{H} : \mathbb{R}^p \rightarrow \mathbb{R}$ is the *hardening energy function*. The *dissipation function* \mathcal{D}^p is defined, in component form, according to

$$\begin{aligned} \mathcal{D}^p &:= - \left(\frac{\partial \psi}{\partial \boldsymbol{\varepsilon}^p} \right)^t \dot{\boldsymbol{\varepsilon}}^p - \left(\frac{\partial \psi}{\partial \boldsymbol{\alpha}} \right)^t \dot{\boldsymbol{\alpha}} \\ &= (\nabla W(\boldsymbol{\varepsilon} - \boldsymbol{\varepsilon}^p))^t \dot{\boldsymbol{\varepsilon}}^p - (\nabla \mathcal{H}(\boldsymbol{\alpha}))^t \dot{\boldsymbol{\alpha}}. \end{aligned} \quad (\text{B.3})$$

The *hyperelastic constitutive equations* and the restriction placed on the dissipation function are obtained by exploiting the second law of thermodynamics in the form of the Clausius–Duhem inequality and, following standard arguments (see [26, 27]), take the form

$$\boldsymbol{\sigma} = \nabla W(\boldsymbol{\varepsilon} - \boldsymbol{\varepsilon}^p) \quad \text{and} \quad \mathcal{D}^p \geq 0, \quad (\text{B.4})$$

where $\boldsymbol{\sigma}$ are the Kirchhoff stress resultant components (cf. (3.8)). Non-negativity of the dissipation function ensures that plastic flow is a dissipative process. Notice that the component expression (B.3)₂, using the notation of Section 3, may be expressed as

$$\mathcal{D}^p = \tilde{\mathbf{J}}\tilde{\mathbf{n}} : \tilde{\mathbf{d}}_e^p + \tilde{\mathbf{J}}\tilde{\mathbf{m}} : \tilde{\mathbf{d}}_i^p - \nabla \mathcal{H}(\hat{\boldsymbol{\alpha}}) : L_v \hat{\boldsymbol{\alpha}}, \quad (\text{B.5})$$

where $\hat{\boldsymbol{\alpha}}$ is resolved in the basis $\{\mathbf{a}^1, \mathbf{a}^2, \mathbf{a}^3\}$ with components $\boldsymbol{\alpha}$.

Thus far the constitutive equations are presented *strain space*; i.e. the response functions

are expressed in terms of the state variables $\{\boldsymbol{\varepsilon}, \boldsymbol{\varepsilon}^p, \boldsymbol{\alpha}\}$. In classical plasticity the response functions, e.g. the yield condition and the flow rule, are formulated in *stress space* in terms of the variables $\tau \in (-\infty, t] \mapsto \{\boldsymbol{\sigma}(x, \tau), p(x, \tau)\}$, where $\boldsymbol{\sigma} \in \mathbb{R}^8$ is a function of $\{\boldsymbol{\varepsilon}, \boldsymbol{\varepsilon}^p\}$ and $p \in \mathbb{R}^p$ denote a complementary set of internal variables which are functions of $\boldsymbol{\alpha} \in \mathbb{R}^p$ through the Legendre transformation

$$\mathcal{H}(\boldsymbol{\alpha}) = -p^t \boldsymbol{\alpha} - \Theta(p), \quad (\text{B.6})$$

where $\Theta : \mathbb{R}^p \rightarrow \mathbb{R}$ is the complementary potential associated with \mathcal{H} . One refers to $\{\boldsymbol{\sigma}, p\}$, which are constrained to lie in the closure of the elastic range E_σ defined in Section 4, as the *fluxes* conjugate to the variables (*affinities*) $\{\boldsymbol{\varepsilon} - \boldsymbol{\varepsilon}^p, \boldsymbol{\alpha}\}$. Typical examples for the functions $\mathcal{H}(\boldsymbol{\alpha})$ and $\Theta(p)$ which fit many classical plasticity models; e.g. J_2 -flow theory, take the form

$$\mathcal{H}(\boldsymbol{\alpha}) = \frac{1}{2} \boldsymbol{\alpha}^t D \boldsymbol{\alpha} \quad \text{and} \quad \Theta(p) = \frac{1}{2} p^t D^{-1} p, \quad (\text{B.7})$$

where D is assumed constant.⁷ By differentiation of the Legendre transformation (B.6) we obtain the relations

$$\dot{\boldsymbol{p}} = -\nabla \mathcal{H}(\boldsymbol{\alpha}) \quad \text{and} \quad \boldsymbol{\alpha} = -\nabla \Theta(p). \quad (\text{B.8})$$

Making use of (B.8), the dissipation function given in (B.3) is expressed in stress space as

$$\mathcal{D}^p[\boldsymbol{\sigma}, p; \dot{\boldsymbol{\varepsilon}}^p, \dot{\boldsymbol{\alpha}}] := \boldsymbol{\sigma}^t \dot{\boldsymbol{\varepsilon}}^p + \dot{\boldsymbol{p}}^t \dot{\boldsymbol{\alpha}}. \quad (\text{B.9})$$

It is shown in Section 5 that use of the Legendre transformation (B.6) as a means of expressing the flow rule and hardening law in stress space has important algorithmic implications, i.e., it preserves *symmetry* of the *algorithmic* consistent elastoplastic tangent moduli.

References

- [1] G. Stanley, Continuum-based shell elements, PhD dissertation, Applied Mechanics Division, Stanford University, 1985.
- [2] J.C. Simo and T.J.R. Hughes, Elastoplasticity and Viscoplasticity: Computational Aspects (Springer, Berlin, 1989).
- [3] J.C. Simo and R.L. Taylor, Consistent tangent operators for rate-independent elastoplasticity, Comput. Methods Appl. Mech. Engrg. 48 (1985) 101–118.
- [4] M.A. Crisfield, On an approximate yield criterion for thin steel shells, Department of the Environment, TRRL Report 658, Crowthorne, Berkshire (Transport and Road Research Laboratory), 1974.
- [5] M.A. Crisfield, Ivanov's yield criterion for thin plates and shells using finite elements, Department of the Environment, TRRL Report 919, Crowthorne, Berkshire (Transport and Road Research Laboratory), 1979.
- [6] A.A. Ilyushin, Plasticity (in Russian) (Gostekhizdat, Moscow, 1948).
- [7] G.S. Shapiro, On yield surfaces for ideally plastic shells, in: Problems of Continuum Mechanics (SIAM, Philadelphia, PA, 1961) 414.
- [8] G.V. Ivanov, Inzh. Zh. Mekh. Tverdogo Tela 74 (6) (1967).
- [9] J.C. Simo, J.G. Kennedy and S. Govindjee, Non-smooth multisurface plasticity and viscoplasticity. Loading/unloading conditions and numerical algorithms, Internat. J. Numer. Methods Engrg. 26 (1988).

⁷ For example, in classical J_2 -flow theory with linear isotropic hardening, $\mathcal{H}(\boldsymbol{\alpha}) = \frac{1}{2} \alpha \kappa' \alpha$ and $\Theta(p) = \frac{1}{2} p(1/\kappa')p$, where $\alpha \in \mathbb{R}$ is the *equivalent plastic strain* and $p \in \mathbb{R}$ is the associated conjugate variable.

- [10] J.C. Simo, J.G. Kennedy and R.L. Taylor, Complementary mixed finite element formulations for elastoplasticity, *Comput. Methods Appl. Mech. Engrg.* 74 (1989) 177–206.
- [11] J.C. Simo and D.D. Fox, On a stress resultant geometrically exact shell model. Part I: Formulation and optimal parametrization, *Comput. Methods Appl. Mech. Engrg.* 72 (1989) 267–304.
- [12] J.C. Simo, D.D. Fox and M.S. Rifai, On a stress resultant geometrically exact shell model. Part II: The linear theory; Computational aspects, *Comput. Methods Appl. Mech. Engrg.* 73 (1989) 53–92.
- [13] J.C. Simo, D.D. Fox and M.S. Rifai, On a stress resultant geometrically exact shell model. Part III: Computational aspects of the nonlinear theory, *Comput. Methods Appl. Mech. Engrg.* 79 (1990) 21–70.
- [14] M. Robinson, A comparison of yield surfaces for thin shells, *Internat. J. Mech. Sci.* 13 (1971) 345–354.
- [15] W.T. Koiter, *Progr. Solid Mech.* 6 (1960).
- [16] G. Maier, A matrix structural theory of piecewise linear elastoplasticity with interacting yield planes, *Meccanica* (1970) 54–66.
- [17] G. Maier and D. Grierson, *Engineering Plasticity by Mathematical Programming* (Pergamon, New York, 1979).
- [18] P. Perzyna, Thermodynamic theory of viscoplasticity, in: *Advances in Applied Mechanics*, Vol. 11 (Academic Press, New York, 1971).
- [19] L.M. Kachanov, *Fundamentals of the Theory of Plasticity* (Mir, Moscow, 1974).
- [20] L. Malvern, *An Introduction to the Mechanics of a Continuous Media* (Prentice Hall, Englewood Cliffs, NJ, 1969).
- [21] T.J.R. Hughes and J. Winget, Finite rotation effects in numerical integration of rate constitutive equations arising in large-deformation analysis, *Internat. J. Numer. Methods Engrg.* 15 (1980) 1413–1418.
- [22] O.C. Zienkiewicz, *The Finite Element Method*, 3rd Edition (McGraw-Hill, London, 1977).
- [23] W. Johnson and P.B. Mellor, *Engineering Plasticity* (Wiley, New York, 1983).
- [24] S. Timoshenko and W. Woinowsky-Kreiger, *Theory of Plates and Shells*, 2nd Edition (McGraw-Hill, New York, 1959).
- [25] P.G. Hodge and T. Belytschko, Numerical methods for the limit analysis of plates, *J. Appl. Mech.* 15 (1968) 796–801.
- [26] B.D. Coleman and W. Noll, The thermodynamics of elastic materials with heat condition and viscosity, *Arch. Rational Mech. Anal.* 13 (1963) 167–178.
- [27] B.D. Coleman and M.E. Gurtin, Thermodynamics with internal variables, *J. Chem. Phys.* 47 (1967) 597–613.
- [28] J.E. Dennis and R.B. Schnabel, *Numerical Methods for Unconstrained Optimization* (Prentice Hall, Englewood Cliffs, NJ, 1983).
- [29] D.G. Luenberger, *Linear and Nonlinear Programming* (Addison-Wesley, Menlo Park, CA, 1984).
- [30] P.M. Naghdi, Stress-strain relations in plasticity and thermoplasticity, in: *Proc. 2nd Symp. on Naval Structural Mechanics* (Pergamon, London, 1960).
- [31] J.C. Simo and R.L. Taylor, A return mapping algorithm for plane stress elastoplasticity, *Internat. J. Numer. Methods Engrg.* 22 (1986) 649–670.